CTCF-mediated Genomic Effects of BART Region on Epstein-Barr Virus Chromatin 3D Structure in Gastric Carcinoma Cells

Kyoung-Dong Kim[1], Subin Cho[2], Taelyn Kim[2], Sora Huh[2], Lina Kim[2], Hideki Tanizawa[3], Jae-Ho Shin[4], Teru Kanda[5], Kyoung Jae Won[6], Paul M. Lieberman[7], Hyosun Cho[8]* and Hyojeung Kang[2]*

[1]Department of System Biotechnolog, Chung-Ang University, Anseong, Korea

[2]Vessel-Organ Interaction Research Center, VOICE (MRC), Cancer Research Institute, College of Pharmacy, Kyungpook National University, Daegu, Korea

[3]Institute of Molecular Biology, University of Oregon, Eugene, Oregon, United States of America

[4]Department of Applied Biosciences, Kyungpook National university, Daegue, Korea

[5]Division of Microbiology, Faculty of Medicine, Tohoku Medical and Pharmaceutical University, Sendai, Japan

[6]Biotech Research and Innovation Centre (BRIC), University of Copenhagen, Copenhagen, Denmark

[7]Program in Gene Expression and Regulation, The Wistar Institute, Philadelphia, Pennsylvania, United States of America

[8]Duksung Innovative Drug Center, College of Pharmacy, Duksung Women's University,

Seoul, Korea

*Corresponding Author: Hyojeung Kang, Kyungpook National University, 80 Daehak-ro, Buk-gu, Daegu 41566, Korea. Phone: 82-53-950-8569; Fax: 82-53-950-8557; E-mail: hkang72@knu.ac.kr, Hyosun Cho, Duksung Women's University, Seoul, Korea. Phone: 82-2-901-8678; Fax: 82-2-901-8386; E-mail: hyosun1102@duksung.ac.kr

Abstract

EBV latent infection in gastric carcinoma (GC) cells is characterized by distinct viral gene expression programs. CCCTC-binding factor (CTCF) is a chromatin structural factor that has been involved in coordinated chromatin interactions between multiple loci of Epstein-Barr virus (EBV) genes. Here, we investigate the role of CTCF in regulating EBV gene expression and chromosome conformation in model of EBV-associated gastric carcinoma (EBVaGC). Chromatin immunoprecipitation followed by sequencing (ChIP-seq) against CTCF revealed 16 CTCF binding sites (BS) in EBV genome of EBVaGC, SNU719 cells. Among the CTCF BSs, one site named as BARTp (BamHI A right transcript promoter) CTCF BS is located at upstream of 11.8-kb BART region (EBV genome: 139724-151554) and was not yet defined its biological functions in EBV life cycle. EBV BART encodes a complex miRNA cluster of highly spliced transcripts that is implicated in EBV cancer pathogenesis. This present study investigated the functional role of the CTCF binding site at BARTp (BARTp CTCF BS) in regulating EBV gene transcription and EBV three-dimensional (3D) genome structure as DNA loop maker. Circular chromatin confirmation capture (4C)-seq and

chromatin confirmation capture (3C)-semi-quantitative(sq)PCR assays using SNU719 cells revealed that BARTp CTCF BS interacts with CTCF BSs of LMP1/2, Cp/OriP, and Qp in EBV genome. We generated mutations in BARTp CTCF BS (S13) in bacmids with ($BART^+$) or without ($BART^-$) the 11.8-kb BART transcript unit (B(+/-)). ChIP-qPCR assay demonstrated that CTCF binding was ablated from BARTp in EBV B(+/-) $S13^-$ genomes (mutant S13), elevated at several other sites such as *LMP1*, *OriP*, and *Cp* in EBV B(-) ($BART^-$) $S13^-$ genome, and decreased at the same sites in EBV B(+) $S13^-$ genome. Infection assay showed that BARTp CTCF BS mutation reduced infectivity, while BART transcript deletion has no detectable effects. Gene expression tests showed that *EBNA1* was highly downregulated in B(+/-) $S13^-$ EBVs related to B(+/-) $S13^+$ EBVs (wild-type S13). *LMP1* and *BZLF1* were more downregulated in B(-) $S13^-$ EBV than B(+) $S13^-$ EBV. Taken together, these findings suggest that the CTCF binding and BART region contribute to EBV 3D genome structure via a cluster of DNA loops formed by BARTp CTCF BS (S13) and are important for coordinated viral gene expression and EBV infectivity.

Introduction

Epstein-Barr virus (EBV) is a member of the human gamma herpesvirus family that establishes lifelong latent infection in the most population [1]. EBV latent infection is associated with lymphoma such as Burkitt's lymphoma (BL) and Hodgkin's lymphoma (HL), and epithelial neoplasm such as nasopharyngeal carcinoma (NPC) and gastric carcinoma (GC) [2, 3]. During the latency phase, EBV genome exists as multicopy episomes that express only a few of viral genes called latent genes [4]. The latency can be changed into the lytic phase depending on developmental stage, environmental signals and pharmacological manipulation

[5, 6]. Approximately 10% GC has been diagnosed as EBV associated gastric carcinoma (EBVaGC), estimating more than 70,000 cases worldwide per year [7-9]. EBVaGC appears lymphoepithelioma-like carcinoma whose definition is an undifferentiated carcinoma with lymphocytic infiltrate, histologically similar to NPC [2, 7]. EBV of EBVaGC maintains the type I latency phase and express the narrowest group of EBV latent genes such as *EBNA1*, *EBER*, BARTs and sometimes *LMP2A*. These genes are implicated with the EBVaGC oncogenesis [10].

The EBV genome contains two miRNA cluster that encoded by BamHI fragment H rightward open reading frame 1 (BHRF1) and BamHI A right transcripts (BARTs) [11-14]. EBV BARTs are a complex miRNA cluster of highly spliced transcripts initially found in NPC EBV strain [15, 16]. Some lymphotropic BL EBV strain, like B95-8, have a deletion overlapping the 11.8-kb BART region (139724-151554), while EBV strains derived from GC, such as GC1 and YCCEL1, contain the full BART region [17, 18]. BART miRNAs are substantially expressed in EBV infected epithelial cells such as NPC and EBVaGC [19-21]. The BART miRNAs are highly implicated in EBV-mediated epithelial malignancies but sometimes dispensable in EBV-mediated lymphoma. Thus, their function in EBV life cycle is only partially elucidated [22].

The maintenance of chromatin structure is also largely dependent on cellular mechanisms that regulate several chromatin interactions exemplified an interaction between enhancer and promoter [23-26]. The CCCTC-binding factor, also referred to CTCF, is a transcription factor that contains DNA binding domain and 11 zinc fingers. CTCF is involved in other functions such as epigenetic insulator, gene boundary factor and DNA looping maker [27-29]. In particular, CTCF is highly associated with regulating long range chromatin

interaction by chromatin loop organization [30]. Cohesin composed of SMC1, SMC3, and non-SMC components including RAD21, SA1, and SA3 are known to assist in CTCF-mediated stabilization of EBV genome structure [31-33]. Cohesion binds at multiple control regions of EBV genes and involves in maintain EBV genome structure to regulate EBV gene expression, along with CTCF [34-36].

Here, we have identified 16 CTCF binding sites (BS) in the EBV genome in EBVaGC using ChIP-seq analysis against CTCF. Among them, one site (BARTp CTCF BS) located in close proximity to the transcription start site of the 11.8-kb BART region that has not yet been defined for its biological function in EBVaGC. This CTCF binding site, referred to here as the BARTp CTCF BS (S13), exits in most EBV genomes regardless of the existence of 11.8-kb BART. Here, we test the hypothesis that the BARTp CTCF BS (S13) is important for 3D conformation of EBV genome, and that the BART transcripts affect this conformation. We further test whether BARTp CTCF BS (S13) regulates EBV gene expression. We find that BARTp CTCF BS (S13) contributes to both BART transcription regulation and 3D conformation, and is likely to contribute to regulation of EBV oncogenesis and life cycle.

Materials and Methods

Cell lines and Reagents

HEK293 cells and HEK293-EBV bacmid cell lines were cultured in Dulbecco's Modified Eagle Medium (DMEM; Hyclone, Pittsburgh, PA, USA) supplemented with 10% Fetal Bovine Serum (FBS; Hyclone, Marlborough, MA, USA), antibiotics/antimycotics (Gibco, Waltham, MA, USA), and Glutamax (Gibco, Waltham, MA, USA) at 37°C, 5% CO_2,

95% humidity in a CO_2 incubator. HEK293 cells were transfected with EBV bacmid and them selected with hygromycin B (400 μg/ml) (Wako, Japan). Gastric carcinoma cell lines SNU719 (EBVaGC) was purchased from Korean Cell Line Bank (Seoul, Korea) and cultured in RPMI 1640 medium (Hyclone, Pittsburgh, PA, USA) supplemented with 10 % FBS, antibiotics/antimycotics and GlutaMAX at 37 °C with 5% CO_2 and 95% humidity.

Microscale thermophoresis (MST) assay

Wild type (Wt) S13 49-mer primer set spanning EBV 138,946~138,956 was designed whose forward primer was labeled with 5-carboxyfluorescein (5-FAM) (Fig. 2A). We in parallel designed mutant (Mt) S13 49-mer set as counterpartner for Wt S13 49-mer primer set. Mt S13 50-mer contains several point mutations in region spanning EBV 138,963~138,987 whose mutations were expected to disrupt CTCF binding to Wt S13 49-mer primer set (Fig. 2A). 10 μl of 100 μM forward Wt S13 49-mer primer was mixed with 10 μl of 100 μM reverse Wt S13 49-mer primer. The mixture was paired by placing it in a thermocycler which programmed to start at 95℃ for 2 min and then gradually cool to 25℃ over 45 min. In parallel, 10 μl of 100 μM forward Mt S13 49-mer primer was also mixed and pared with 10 μl of 100 μM reverse Wt S13 49-mer primer. Resultant paired both Wt and Mt (Wt/Mt) S13 49-mer primer sets were used as target DNA in MST assay. Using baculovirus expression system, his-tagged CTCF proteins were purified from Sf9 cells transfected with CTCF expression plasmid. Resultant CTCF proteins were used as ligand protein in MST assay. To make CTCF bind to Wt/Mt S13 49-mer primer sets, reaction mixture

was prepared as followed: 5 ul 4X EMSA buffer (400 mM KCl, 80 mM HEPES, 0.8 mM EDTA, 80% glycerol, pH 8.0) freshly added 1 mM DTT, target DNA (125 nM), 1 ul 500 ng/ul sonicated salmon sperm DNA, 2.5 ul ligand protein (CTCF, 3.12 μM, 6.25 μM), and 8.5 ul sterile water. Afterward, each mixture was incubated 30 min on ice and subjected to Nanotemper Monolith NT.115 (Munich, Germany) as recommended by manufacturer.

PCR

To confirm BART region in EBV genome, PCR was performed at BART region using each EBV BART^{+} (B(+)) and EBV BART^{-} (B(-)) S13^{-} bacmids. One directional primers were used to avoid the amplication for self-ligation products; primers for PCR products of BART region from EBV B(+) Wt bacmid were used the forward primer. Each 25μl reaction contained 5 μl of EBV B(+) and B(-) Wt bacmid templates, 5 μl of 5× reaction mix (NanoHelix, Korea), 5 μl of 5× TuneUp solution (NanoHelix, Korea), 1 μl of Taq-plus polymerase (NanoHelix, Korea), and 2.5 μl of 10 μM forward/reverse primer. The following cycle conditions were used: 95°C for 3 min; 30 cycles of 95°C for 30 s, 55°C for 30 s, and 72°C for 30 s; followed by 72°C for 10 min. The reactions were performed using a TaKaRa PCR Thermal Cycler (Otsu, Japan) and then run on a 1.5% agarose/TBE gel.

Real-time quantitative PCR (qPCR)

Quantification of precipitated DNA was determined using real-time quantitative PCR (qPCR) with SYBER Green in FastStart Essential DNA Green Master (Roche, Basel, Switzerland). Each resultant DNA was diluted in nuclease-free water and was analyzed in

triplicated for EBV-associated genes and CTCF binding sites. The PCR reaction mixture of 20 µl contained 5 µl of template DNA, 0.5 µM of each primer and 10 µl of Master Syber Green 1 mix (Roche, Basel, Switzerland). The Primer sequences listed in Table 1. The following cycles thermal conditions were used: 95°C for 10 min; 45 cycles of 95°C for 10 sec, 55°C for 10 sec, and 72°C for 10 sec; 95°C for 5 sec; followed by 65°C for 1 min. In case of necessity, semi-quantitative PCR (sqPCR) was also conducted as previously described [37]. PCR products were amplified in a 25 µL reaction solution containing 5 µL of 5× reaction mix, 5 µL of 5× TuneUp solution, 1 µL of Taq-plus polymerase, and 2.5 µL of 10 pmol forward/reverse primer. The following cycle conditions were used: 95◦C for 3 min; 30 cycles of 95 ◦C for 10 s, Tm (specific to primer sets) for 30 s, and 72 ◦C for 30 s; followed by 72 ◦C for 10 min. The reactions were performed using a TaKaRa PCR Thermal Cycler (TaKaRa, Kyoto, Japan) and then run on a 1.2% agarose/TBE gel.

Construction of recombinant EBV bacmid

Site-directed mutations were introduced at BARTp CTCF BS (S13) in EBV B(+) or B(-) (B(+/-)) bacmids to make EBV B(+/-) S13^{-} bacmids that contains mutation in BARTp CTCF BS. EBV B(+) are isogenic and made from EBV B(-)bacmid [38]. EBV B(+/-) S13^{-} bacmids were generated using two-step red-mediated recombination method. Primers for PCR products of the kanamycin resistant gene (Kan^{r}) from pEPKanS3 plasmid used the forward primer 5'-GCA TCT TTC TAA CCA GTA GGG GCC TCC ACC TAG GTG CTT TGT TAA TCT TTA GTG TAT ATA TAT ATA TAT ATA TAT ATA TGG GTA CCC CTA TCC TAC AAC CAA TTA ACC AAT TCT GAT TAG-3'and the reverse primer 5'-ACA GGG ATT ATC AAG ACA AGG AGC TCC GGT AGG ACC TAT AGG ATA GGG

GTA CCC ATA TAT ATA TAT ATA TAT ATA TAT ACA CTA AAG ATT AAC AAA GGA TGA CGA CGA TAA GTA GGG ATA- 3'. Resultant PCR products were composed Kan^r gene with I-SceI site, flanked by 60 bp downstream and upstream of EBV BARTp CTCF BS sequence surrounding the designed CTCF mutation sequence. These PCR products were electroporated into GS1783 competent cells containing EBV B(+/-) $S13^+$ bacmids for 1st round homologous recombination. EBV B(+/-) $S13^-$ bacmid with Kan^r gene was recovered by positive selection, characterized by restriction enzyme digestion and transformed into GS1783 I-SceI-inducible competent cells. Kan^r gene was removed from EBV bacmid-Kan^r by 2nd round homologous recombination and negative selection to make complete EBV B(+/-) $S13^-$ bacmids. Final CTCF mutation was confirmed by restriction enzyme digestion and DNA sequencing of the homologous recombination site in EBV B(+/-) $S13^-$ bacmids.

Transfection

EBV B(+/-) $S13^{+/-}$ (B(+)$S13^+$, B(+)$S13^-$, B(-)$S13^+$, B(-)$S13^-$) bacmids were transfected into HEK293 cells using Neon transfection system (Invitrogen, Carlsbad, CA, USA). 5 x 10^4 cells were resuspended in 100 µl of serum-free media containing 5ug of each mutant recombinant bacmid. The electroporation was conducted with Neon electroporator (Invitrogen) set at 1350 V, 30 ms and 1 pulse. Cells were placed in media supplemented with 10% FBS for 48 h post-transfection.

Western blotting assay

Western blotting was performed in HEK293-EBV B(+/-) $S13^{+/-}$ (B(+)$S13^+$, B(+)$S13^-$,

B(-)S13^{+}, B(-)S13^{-}) cells. Cells (5 × 10^{6}) were then lysed using 100 µl of RIPA lysis buffer (Promega, WI) supplemented with 1 µl of proteinase inhibitor and 10 µl of phenylmethylsulfonylfluoride. The cell lysates were further fractionated using the Bioruptor sonicator (5 min, 30 sec on/off pulses). Cell lysates were loaded onto 8% sodium dodecyl sulfate polyacrylamide electrophoresis gel and subjected to Western blot analysis by using antibodies against EBV proteins (1:1000 dilution). Following antibodies were used: anti-EBV EBNA1 (Santa Cruz Biotechnology (SCB), Santa Cruz, CA, USA), anti-EBV BZLF1 (SCB), EA-D (SCB), anti-LMP1 (SCB) and anti-GAPDH (Cell Signaling Technology, Danvers, MA, USA), Horseradish peroxidaseconjugated sheep anti-mouse IgG (Genetex, Irvine, CA, USA), horseradish peroxidase conjugated donkey anti-rabbit IgG (Genetex), and horseradish peroxidase-conjugated goat anti-rat IgG (Bethyl Laboratories, Montgomery, TX, USA) were used as secondary antibodies.

Immunofluorescence Assay

HEK293-EBV B(+/-) S13$^{+/-}$ (B(+)S13^{+}, B(+)S13^{-}, B(-)S13^{+}, B(-)S13^{-}) cells were grown on coverslips in 24-well plates (2 × 10^{5}/well). Next day, cells were fixed with 4 % paraformaldehyde for 30 min and were permeabilized with 0.25 % Triton X-100 in PBS for 90 min. Treated cells were blocked using 1 % BSA in PBS containing 0.1 % Tween 20 for 60 min. Sample were stained with EBNA1 antibody (1 : 40). After overnight incubation at 4 °C, coverslips were washed 3X in PBS and treated with Alexa-594 (Thermo Fisher Scientific, Waltham, MA) for 2 h at 4 °C. Alexa-594 was used to detect EBNA1. After washing 3X in PBT (PBS containing 0.5 % Triton X-100), coverslips were mounted with DAPI (SouthernBiotech, Birmingham, AL). Samples were analyzed using immunofluorescence

confocal microscopy.

CTCF ChIP-seq analysis

ChIP-seq against CTCF was performed with 5 x 10^7 SNU719 cells per sample and crosslinked using formaldehyde. Crosslinked SNU719 cell lysates was sonicated to achieve a DNA fragment length of ~ 100 – 500 bp. Immunoprecipitation was carried out was carried out with 10 µg of either rabbit anti-CTCF (Millipore, Burlington, MA, USA) or control rabbit IgG (SCB), incubated overnight with antibody-coated Dynabeads protein A/G (Invitrogen). Incubated beads were washed with ChIP-seq wash buffer (50 mM HEPES, pH 7.5, 500 mM LiCl, 1 mM EDTA, 1% NP-40, 0.7% Na-Deoxycholate, 1x protease inhibitors) for 5 times, then washed once with 50 mM NaCl in TE buffer. Immunoprecipitated DNA was eluted with ChIP-seq elution buffer (50 mM Tris-HCl, pH 8, 10 mM EDTA, 1% SDS), reverse-crosslinked at 65°C, treated with RNase A (0.2 mg/ml) and proteinase K (0.2 mg/ml), purified with phenol and chloroform, then subjected to qPCR validation. Validated ChIP samples were isolated by agarose gel purification, ligated to primers, and then subject to Illumina-based sequencing using manufacturer's protocol (Illumina, San Diego, CA, USA). ChIP-seq reads were mapped to the EBV wide-type reference genome (NC 007605) using Bowtie. For peak calling findPeaks command in Homer software was applied [39].

ChIP assay

CTCF or Cohesin ChIP assays were performed with 3 x 10^6 SNU719 cells or HEK293-EBV B(+/-) $S13^{+/-}$ (B(+)$S13^+$, B(+)$S13^-$, B(-)$S13^+$, B(-)$S13^-$) cells per sample according to the cross-linking chromatin immunoprecipitation (X-ChIP) protocol provided by

Abcam (Cambridge, UK) with a slight modification. The Bioruptor (BMS, Korea) was used to sonicate genomic DNA according to the manufacturer's protocol. Sonicated cell lysates were subjected to immunoprecipitation with antibodies to CTCF (Millipore), SMC1 (Bethyl Laboratories, Montgomery, TX, USA), SMC3 (Bethyl Laboratories) and normal rabbit IgG (SCB). The precipitates were incubated with ChIP elution buffer (1% SDS, 100 mMNaHCO3); then the samples were reverse-crosslinked at 65°C overnight and purified on Promega columns. The purified DNA was analyzed using RT-qPCR. ChIP values were calculated as fold increases over the isotype specific IgG values for each primer sets.

3C and 4C-seq assays

Chromatin confirmation capture (3C) and circular chromatin confirmation capture (4C)-seq assays were performed as previously reported [40]. Briefly, 1 x 10^7 SNU719 cells were fixed in 1% paraformaldehyde for 10 min at 37 °C. Nuclei were permeabilized by incubation with 0.5% SDS at 62 °C for 10 min. A half of DNA was digested with 100 units of *XhoI* (New England Biolabs (NEB), Ipswic, MA, USA) and ligated in the nucleus followed by in situ 3C protocol [41]. Other half of DNA was digested with 100 units of MboI (NEB) and ligated in the nucleus followed by in situ Hi-C protocol [42]. After reversal of crosslinks, 3C DNA was prepared and examined the association between two genomic loci by using 3C primers. For 4C-seq, DNA was digested with 100 units of MboI (NEB) and ligated in the nucleus followed by in situ Hi-C protocol [42]. 3C DNA was further digested with 100 units of Csp6I (NEB) and re-ligated. For each primer viewpoint, a total 10 to 100 ng DNA was amplified by PCR. All samples were sequenced with NovaSeq 6000 100 bp paired read. 4C-seq experiments from all viewpoints were carried out in biological replicates for SNU719

cells.

4C-seq data analysis

The 100-bp sequence paired-end reads were trimmed and grouped by cutadapt (version 2.10) based on the sequence from 4C bait location. Reads were aligned to EBV genome (NC_007605) using Bowtie2 (version 2.2.3) with iterative alignment strategy. Reads with low mapping quality (MapQ < 10) and reads that mapped to human repeat sequences were removed. Total aligned reads for each *i*-th position of non-overlapping 10-kb window (N_i) were calculated. Then, converted to the *P*-values using the Poisson formula:

$$Pi=1-\sum j=0Ni\lambda e-\lambda/j!Pi=1-\sum j=0Ni\lambda e-\lambda/j! \quad (1)$$

where λ is equal to the average of reads for each 10-kb window (except EBV aligned reads). The significant peaks were defined using subcommand bdgpeakcall of MACS2 software (version 2.1.1) with parameters: at least *P*-value < 10^{-5} (option -c 5), minimum length of 20-kb (option -l 20000) and maximum gap of 10-kb (option -g 10000). Total significant peak number for each 10-kb of bait positions (2 BART, FR, DS/Cp, Qp, LMP) were counted.

EBV infection study

6.3 x 10^5 HEK293-EBV B(+/-) $S13^{+/-}$ (B(+)$S13^+$, B(+)$S13^-$, B(-)$S13^+$, B(-)$S13^-$) cells were seeded on 6-cm culture dish. On next day, HEK293-EBV B(+/-) $S13^{+/-}$ cells were transfected with pCDNA3-BZLF1 and pCDNA3-BALF4 using TurboFect Transfection

Reagent (Thermo Scientific, Waltham, MA, USA). Old medium was changed with fresh medium in one day post transfection. Medium was harvested in three days post transfection. Harvested medium was then clarified by twice centrifugation at 3000 rpm and once filtering with 0.45 μL filter (Sartorius stedium biotech, Gottingen, Germany). Next, 3 x 10^5 HEK293 cells were plated on a well of 6-well culture plate. In next day, old medium was removed from the HEK293 cells. 40 μm cell strainer (FALCON, Corning, NY, USA) was loading on the HEK293 cells and refilled with the clarified old medium harvested from HEK293-EBV B(+/-) $S13^{+/-}$ cells. EBV infection was occurred from the clarified medium to HEK293 cells through cell strainer for 24 h.

Statistical Analysis

Statistical tests were performed using unpaired t-test and ANOVA. P-values (one-tailed) <0.05 (95% confidence) were considered statistically significant.

Results

Distribution of CTCF binding site (BS) in $BART^+$ EBV genome

ChIP-seq was performed to identify CTCF BS in the EBV genome of EBVaGC SNU719 cells. The sequencing reads were mapped to the EBV reference genome (NC_007605) and were visualized using the Homer tools [39]. Approximately 5.7×10^4 CTCF ChIP reads and 2.7×10^6 IgG reads were aligned to EBV reference genome sequence and displayed reads on EBV genome using UCSC genome browser (Fig 1A). Enrichment of

315 CTCF ChIP products relative to IgG ChIP products was calculated and visualized as the lower
316 bound of 95% confidence. 16 high-confidence peaks were identified based on a read depth.
317 CTCF binding sites were enriched at *BNRF1* (S1), *BCRF1* locus (S2), *BPLF1* locus (S5),
318 *BMRP1* locus (S8), *BRLF1* locus (S11), *BART* (*RPMS1*) locus (S13), and *LMP1/2* locus (S16).
319 These peaks were located in control regions of EBV genes such as upstream or downstream
320 of their transcriptional start sites. One peak, S13 is located close to the BART promoter region
321 and within the intro of *RPMS1* gene. Given to its locations, we speculate that this CTCF
322 binding site (S13) functions as a transcriptional regulator and/or DNA loop maker, which
323 mediate transcriptional regulator via chromatin interactions in EBV genome. To confirm
324 CTCF BSs identified from ChIP-seq analysis in SNU719 cells, we performed ChIP-qPCR
325 assays with CTCF and cohesion antibodies in these same cells. Since cohesins often
326 colocalize with CTCF sites [32], we also assayed cohesion binding at these sites (Fig. 1B and
327 1C). CTCF and SMC1 strongly bound to most (four sites among tested five sites) CTCF BSs
328 identified from ChIP-seq, while SMC3 was weakly bound to the CTCF BSs tested. In
329 particular, CTCF and cohesins were more strongly recruited to S13 compared with other
330 tested regions except S16. Taken together, all these results speculated that CTCF bound to
331 S13 is likely to play dominant roles in chromatin interactions for EBV gene regulation in
332 SNU719 cells.

333

334 **The CTCF binding site in BART promoter region**

335 Functional roles of CTCF BSs in EBV genome have been identified in EBV-
336 associated lymphoid cells, such as Mutu I, Mutu-LCL, and Raji. CTCF BSs such as S1, S2,
337 S5, and S16 in Fig.1A were characterized in previous studies and implicated in forming

looping structure [41, 43, 44]. However, S13 (BARTp CTCF BS) was not previously characterized. To understand the role of CTCF binding at S13, we first validated that S13 bound directly to a CTCF protein from Sf9 cells using baculovirus CTCF expression system (Fig. 2B). To validate the specific sequence recognition site for CTCF, we used site-directed mutation to introduce mutations predicted to disrupt CTCF binding to S13 (Fig. 2A). We conducted microscale thermophoresis (MST) assay to confirm CTCF binding to wild-type (Wt) S13 and mutated (Mt) S13 DNA fragments (Fig. 2C). We observed strong binding of CTCF to Wt S13 DNA fragments that were significantly compromised for binding to Mt S13 DNA fragments (Fig. 2C lower panel). As control, total proteins isolated from Sf9 cells showed no strong selectivity in binding to Wt S13 or Mt S13 DNA fragments (Fig. 2C upper panel). These data indicated that Wt S13 is a good target site for CTCF binding and suitable for BARTp CTCF BS.

Chromatin interaction between CTCF BS in BART^{+} EBV genome

To examine if BARTp CTCF BS (S13) is required for the formation of DNA looping structure, 4C-seq was conducted at around BARTp CTCF BS in SNU719 cells. Nucleus isolated from SNU719 cells were permeabilized, DNA-digested, and ligated to make 4C-seq products. Amplicons of 4C-seq products from view point primers were sequenced followed by aligning resultant sequencing reads to EBV genome (Fig. 3A). This 4C-seq data showed that the specific CTCF BS at S13 was involved in several chromatin interactions with multiple loci (Fig. 3B and 3C). Since CTCF binding site S14 is also located in the BART locus, we included S14 interactions along with S13. We found that BARTp CTCF BS (S13-S14, *RPMS1*) interacted strongly with several regions of the EBV genome, including regions

361 at the EBV genome coordinates 5-kb region (S1, *BNRF1*=TP), 45-kb region (S4, *BPLF1*),
362 105-kb region (S12, *BKRF4*), and 155-kb regions (S15, *BALF4*) on the EBV genome. In
363 particular, BARTp CTCF BS showed relatively strong interactions with both 45-kb region
364 (S4) and 105-kb region (S12) except neighboring 155-kb region (S15). We also assayed
365 interactions with other EBV regulatory elements using 4C-seq. OriP CTCF BS (S2) showed
366 the strongest interactions its neighboring region at 5-kb (S1) and at 45-kb (S4). Qp CTCF BS
367 (S5) interacted strongly with 145-kb region (S14), and LMP1/2 CTCF BS (S16) showed the
368 strongest interaction with 55-kb region (S6). Duplicate experiments produced highly
369 reproducible findings (Fig. 3C). These mutual chromatin interactions were depicted as a
370 simple diagram (Fig. 3D). These results indicated that CTCF sites mediate DNA interactions
371 throughout the EBV genome, and that BARTp CTCF BS intensively forms a cluster of several
372 DNA loops with other important loci in the EBV genome of SNU719 cells.

373

374 **Confirmation of chromatin interactions mediated BARTp CTCF BS**

375 3C assay was conducted to consolidate diverse chromatin interactions identified by
376 4C-seq. Nucleuses isolated from SNU719 cells were subjected to paraformaldehyde-fixation,
377 *XhoI*-digestion, T4 DNA ligase-ligation, and (nested) PCR. BARTp CTCF BS was included
378 in an EBV DNA fragment cut by *XhoI* at 135,936 bp (135K, S13) and 147,676 bp (147K,
379 S14) in EBV genome. Both ends of the 135K-147K DNA fragment were used as view point
380 primers in PCR with 3C products (Fig. 4A). A view point primer designed from 147K (S14)
381 in forward direction was first tested for chromatin interactions with other important loci in
382 EBV genome (Fig. 4B). 147K (S14) locus could clearly interact with 3K (S1, *BNRF1*), 49K
383 (S5, *BFRF3*), and 167K (S16, *LMP1/2*) loci. A second view point primer designed from 135K

(S13) in reverse direction was found to interact with 65K (S8, BORL2) and 167K (S16, LMP1/2) loci. All chromatin interactions were summarized in table (Fig. 4D) and simply depicted as a simple diagram (Fig. 4E). Taken together, all these 3C data indicated that BARTp CTCF BS is involved in forming a cluster composed of at least three DNA loops with OriP CTCF BS (S2), Qp CTCF BS (S5), and LMP1/2 CTCF BS (S16), respectively.

Establishment of HEK293-EBV BART^{-} and BART^{+} BARTp CTCF BS mutant cells

EBV B(+) and B(-) (B(+/-)) genome sequences were compared in previous study [45]. This comparison revealed both loss of 11.8-kb BART region in EBV B(-) genome still retained the BARTp CTCF BS (S13) similar to EBV B(+) genome (Supplemental Fig. 1A). As BARTp CTCF BS is located in *RPMS1* intron region, an introduction of site-directed mutation in BARTp CTCF BS would not affect the *RPMS1* expression (Supplemental Fig. 1B). Resultant EBV B(+) S13^{-} bacmid from red-recombination was confirmed the site-directed mutation in BARTp CTCF BS by Sanger DNA sequencing (Supplemental Fig. 1C). In parallel, EBV B(-) S13^{-} bacmid was also confirmed the mutation by Sanger DNA sequencing (data not shown). Thereafter, EBV B(+/-) S13$^{+/-}$ (B(+)S13^{+}, B(+)S13^{-}, B(-)S13^{+}, B(-)S13^{-}) bacmids were further tested their stabilities by EcoR1-digestion. Using these methods, we did not find any additional loss of EBV DNA (Supplemental Fig. 1D), nor defects in their ability to express GFP after several passages (Supplemental Fig. 1E).

Effects of BARTp CTCF BS mutation on EBV infection

EBV B(+/-) S13$^{+/-}$ (B(+)S13^{+}, B(+)S13^{-}, B(-)S13^{+}, B(-)S13^{-}) bacmid genomes were

406 tested for their EBV infectivity to HEK293 cells. To this aim, HEK293-EBV B(+/-) $S13^{+/-}$
407 cells were transfected with pcDNA3-BZLF1 and pcDNA3-BALF4. B(+/-) $S13^{+/-}$ EBVs were
408 harvested three days post transfection (Fig. 5A). Harvested viruses were tested their
409 infectivity to HEK293 cells as mentioned above (Fig. 5B and 5C). Interestingly, both B(+)
410 $S13^{-}$ and B(-) $S13^{-}$ EBVs were severely defected in their infectivity to HEK293 cells,
411 compared to B(+) and B(-) $S13^{+}$ EBVs. Furthermore, B(-) $S13^{+}$ EBV persisted longer in
412 HEK293 cells than B(+) $S13^{+}$ EBVs. Taken together, these results indicated that BARTp
413 CTCF BS, not the BART transcript, is required to maintain a full capacity of EBV
414 infectivity.

415

416 **Effects of BARTp CTCF BS mutation on EBV gene expression**

417 We further investigated overall expression patterns of EBV genes in HEK293-EBV
418 B(+/-) $S13^{+/-}$ (B(+)$S13^{+}$, B(+)$S13^{-}$, B(-)$S13^{+}$, B(-)$S13^{-}$) cells. The mRNA levels of *EBNA1*,
419 *LMP2*, *BZLF1* were significantly lower in B(+/-) $S13^{-}$ EBVs than B(+/-) $S13^{+}$ EBVs (Fig. 6A
420 and 6B). Consistently, the protein levels of *EBNA1*, *LMP2*, *BZLF1* were significantly lower
421 in B(+/-) $S13^{-}$ EBVs than B(+/-) $S13^{+}$ EBVs (Fig. 6C and 6D). Intracellular *EBNA1*
422 expression was also weaker in B(+/-) $S13^{-}$ EBVs than B(+/-) $S13^{+}$ EBVs which were
423 visualized by immunofluorescence assay (Fig. 6E). Taken together, these results indicated
424 that BARTp CTCF BS is required to maintain appropriate expression levels of EBV genes
425 during their latent infection.

426

427 **Effect of 11.8-kb BART region on CTCF enrichment around BARTp CTCF BS**

Given the location of 11.8-kb BART region, we tested if 11.8-kb BART region can make regulatory effect to enrich CTCF on BARTp CTCF BS (S13) surrounding regions. For this aim, CTCF ChIP assay was performed to verify spatial effect of the BART region on the CTCF BSs to EBV genome. HEK293-EBV B(+/-) $S13^{+/-}$ (B(+)$S13^{+}$, B(+)$S13^{-}$, B(-)$S13^{+}$, B(-)$S13^{-}$) cells were subjected to CTCF ChIP assay whose products were analyzed by real-time qPCR assays. As expected, CTCF was almost completely deprived from BARTp CTCF BS in B(+/-) $S13^{-}$ EBVs (Fig. 7A and 7B). Interestingly, in other CTCF BSs surrounding BARTp CTCF BS, CTCF was differently distributed between B(+) $S13^{-}$ EBV and B(-) $S13^{-}$ EBV (Fig. 7A and 7B). Compared to B(+/-) $S13^{+}$ EBVs, CTCF was further enriched at other CTCF BSs around OriP (S2) and LMP1/2 (S16) in B(-) $S13^{-}$ EBV, while CTCF was severely deprived at those sites in B(+) $S13^{-}$ EBV. These ChIP products were further analyzed to reconfirm CTCF distribution by semi-quantitative (sq) PCR assay (Fig. 7C and 7D). It was also observed that the enrichment and deprival of CTCF occurred at CTCF BSs around OriP and LMP1/2 dependent on absence and presence of BART, respectively. Taken together, these results from ChIP-(s)qPCR assays indicated that 11.8-kb BART region plays an important role in enriching CTCF at other CTCF BSs surrounding BARTp CTCF BS to regulate appropriate EBV genome 3D structure.

BARTp CTCF-mediates chromatin interactions

Since BARTp CTCF BS (S13) was implicated to differently distribute CTCF on its surrounding CTCF BSs, we tested whether BARTp CTCF BS might play a regulatory role in forming a cluster of several DNA loops mediated by BARTp CTCF BS. To this aim, 3C-sqPCR assays with HEK293-EBV B(+/-) $S13^{+/-}$ (B(+)$S13^{+}$, B(+)$S13^{-}$, B(-)$S13^{+}$, B(-)$S13^{-}$)

cells were conducted to consolidate chromatin interactions in similar way previously done with SNU719 cells in Fig. 4. Nuclei isolated from HEK293-EBV B(+/-) $S13^{+/-}$ cells were subjected to 3C-sqPCR assay. Multiple chromatin interactions mediated by BARTp CTCF BS with loci such as OriP, Qp, and LMP1/2 were confirmed in HEK293-EBV B(+/-) $S13^{+}$ cells (Fig. 8A). Like SNU719 cells, it was observed that 147K (S14) interacts with 3K (S1) and 167K (S16) regardless of 11.8-kb BART region. In spite of this similarity, both 167K-147K and 65K-147K interactions were slightly stronger in B(+) $S13^{+}$ EBV and B(-) $S13^{+}$ EBV. However, the site-directed mutation in BARTp CTCF BS caused to disrupt most chromatin interactions observed in B(+/-) $S13^{+}$ EBVs (Fig. 8B). However, B(+/-) $S13^{-}$ EBVs could not maintain almost the whole chromatin interactions directly associated with BARTp CTCF BS (Fig. 8B). The B(+/-) $S13^{-}$ EBVs were not observed a specific chromatin interaction such as 65K (S8)-147K(S14). In spite of severe loss of chromatin interactions, some chromatin interactions indirectly associated with BARTp CTCF BS was relatively less affected in B(-) $S13^{-}$ EBV. These indirectly associated chromatin interactions such as 3K-167K and 65K-147K were maintained in B(-) $S13^{-}$ EBV although those interactions were abolished in B(+) $S13^{-}$ EBV (Fig. 8B). All tested chromatin interactions were summarized in table (Fig. 8C) and depicted as simple diagrams (Fig. 8D). Given these data, BARTp CTCF BS (S13) could centralize key chromatin interactions among OriP, Qp, and LMP1/2. The 11.8-kb BART region could make structural effects on forming a key DNA loop cluster via BARTp CTCF BS-mediated chromatin interactions.

Discussion

Gene regulation requires integration of various signals and coordination of these signals across the genome. EBV gene expression is controlled at multiple levels, including transcription factor binding, transcription initiation and elongation, RNA processing, and epigenetic modification that control latent and lytic transcription [6]. In each of these context, CTCF-mediated chromatin interaction has played key roles in regulating EBV gene expression. CTCF BSs at *OriP* (S2 [46]), *Qp* (S5 [41]), and *LMP1/2* (S16 [43]) have been characterized their functional roles in regulating EBV gene expression. Most of these previous studies focused on EBV genomes in Burkitt's lymphoma (BL) or lymphoblastoid cell lines (LCLs). Although 11.8-kb BART region was well conserved in EBV-associated Raji, Mutu, and GC1 cells, few genetic studies were conducted to define miRNAs in 11.8-kb BART region [38]. In particular, BARTp CTCF BS (S13) in gastric carcinoma cells has not been characterized its functional roles in regulating EBV gene expression.

Here, we first showed that BARTp CTCF BS (S13) can form a cluster of DNA loops via chromatin interactions mediated with several CTCF BSs such as *OriP*, *Qp*, and *LMP1/2*. Secondly, we found that functional BARTp CTCF BS (S13) is required to make a stable DNA loop between *OriP* and *LMP1/2*. Thirdly, we showed that BARTp CTCF BS (S13) is an important site of transcriptional regulation of EBV genes such as *EBNA1* and *BZLF1*. Finally, we found that functional BARTp CTCF BS (S13) is necessary for a full capacity of EBV infection. These findings suggested that BARTp CTCF BS (S13) coordinates EBV gene expression via forming interactions with other CTCF BSs in the viral genome.

CTCF has been previously implicated with cohesins in chromatin interactions by forming DNA loops [47]. Long-distance DNA interactions are essential to mediate communication between promoter and enhance elements. EBV OriP has been implicated as a

496 transcriptional enhancer of *Cp* and *LMP1* promoter whose mechanism was to use the CTCF-
497 mediated DNA loop structure [48]. In the present study, we examined the role of CTCF at the
498 BARTp (S13) using EBV-associated gastric carcinoma cells and EBV infected HEK293 cells.
499 We found that deletion of the BARTp CTCF BS (S13) in B(-) EBV genome resulted in more
500 enrichment of CTCF at CTCF BSs in *OriP* and *LMP1/2*, while the deletion in B(+) EBV
501 caused to deprive almost all the CTCF from CTCF BSs in *OriP* and *LMP1/2*. In similar
502 context, the chromatin interactions of *OriP* and *LMP1/2* was more severely defected in EBV
503 B(+) S13$^-$ genome than EBV B(-) S13$^-$ EBV genome due to the differential distribution of
504 CTCF. These results suggested that 11.8-kb BART region could make spatial effects on
505 forming CTCF-mediated DNA loops of *OriP* and *LMP1/2* loci.

506 Taken together, these results suggested that BARTp CTCF BS (S13) can play a
507 complex role in regulating epigenetic modifications at both BART region and its surrounding
508 regions such *LMP1/2* locus and *OriP* locus. One possible function of CTCF at the BARTp is
509 to link *LMP1/2* locus, *OriP* locus, and *Qp* locus into a cluster of DNA loops. This genomic
510 clustering would partly account for the role of CTCF in maintaining EBV latent infection.
511 Similar to this present study, we previously observed that the chromatin interaction between
512 *LANA* locus and *RTA* locus could occur to form a chromatin complex via CTCF during KSHV
513 latent infection. In KSHV, these CTCF-mediated interactions were disrupted during KSHV
514 lytic reactivation [49]. However, for EBV it is not yet known whether CTCF binding and
515 genome conformation change during EBV latent-lytic switch.

516 CTCF has been implicated as a chromatin insulator and boundary factor [50, 51].
517 CTCF can prevent epigenetic drift by blocking heterochromatin formation at the EBV *Qp*
518 region [41]. Deletion of CTCF BS in *LMP1/2* resulted in disrupting *OriP* and *LMP1/2* locus

519 interaction, an increase in histone H3K9me3 and DNA methylation at LMP1 promoter region,
520 and severe reduction of EBV latent infection [43]. In the present study, the deletion of CTCF
521 BS in BARTp (S13) resulted in loss of *EBNA1* and *BZLF1* in mRNA and protein levels. In
522 addition, the deletion caused to severely reduce EBV latent infection regardless of presence
523 of 11.8-kb BART region. Thus, phenotype of BARTp CTCF BS (S13) mutant EBVs was
524 similar to that of *LMP1/2* CTCF BS mutant EBV. One of possible mechanism is that BARTp
525 CTCF might work together with *LMP1/2* CTCF to block the spread of heterochromatin that
526 might be generated by GC-rich respective DNA of the EBV terminal repeat (TR) region.
527 However, it remains to further study molecular mechanism that BARTp CTCF uses to
528 coordinate with *LMP1/2* CTCF in blocking the spread of heterochromatin for EBV gene
529 expression.

530 Recent studies using Hi-C methods examined EBV interactions with host
531 chromosome in various cell types [40, 52]. Another related study used capture Hi-C to analyze
532 KSHV looping DNA interactions during latency and reactivation, and found that DNA loops
533 organized around highly active RNA polymerase II promoters, especially that for the viral
534 PAN non-coding RNA [53]. In the present study, we used Hi-C method to define DNA
535 looping interactions within EBV genome in EBVaGC and focused on the regions controlling
536 the BART transcripts. Similar to KSHV PAN promoter, we found the EBV BART promoter
537 to be an organizing hub for the EBV genome. While we did not examine RNA pol II binding,
538 our findings indicate that CTCF-mediated chromatin interaction is likely to account for most
539 DNA loops within EBV genomes. It is also possible that EBV association with host
540 chromosome may also contribute to some aspects of EBV chromosome conformation.
541 Although our high-resolution 4C analysis did reveal extensive conformational structure of

542 EBV genome during EBV latency in EBVaGC, further studies will be required to resolve
543 some of these more complicated functions of CTCF and to better understand how EBV has
544 exploited CTCF binding sites to confer coordinate gene regulation and genome propagation
545 in latent infection.

546

547 Disclosure of Potential Conflicts of Interest

548 No potential conflicts of interest were disclosed by all authors.

549

550 Author's Contributions

551 Conception and design: H. Kang, H, Cho, S.

552 Development of methodology: H. Kang, K. Kim

553 Acquisition of data (provided animals, acquired and managed patients,
554 provided facilities, etc.): H. Kang, K. Kim, S. Cho, T. Kim, S. Huh, L. Kim

555 Analysis and interpretation of data (e.g., statistical analysis, biostatistics,
556 computational analysis): H. Kang, H. Cho, H. Tanizawa, J. Shin, Kyoung Jae Won

557 Writing, review, and/or revision of the manuscript: H. Kang, H. Cho, P. Lieberman

558 Administrative, technical, or material support (i.e., reporting or organizing
559 data, constructing databases): T. Kanda, P. Lieberman

560 Study supervision: H. Kang, H. Cho

Grant Support

This work was supported by 1) grants from the National Research Foundation of Korea (2018R1D1A3B07045094, 2019R1I1A3A01059629), 2) a grant from the Priority Research Centers Program through the National Research Foundation funded by the Korean Ministry of Education, Science, and Technology (2016R1A6A1A03007648), 3) a grant from the National Research Foundation of Korea grant funded by the Korean Governent(MSIT) (2020R1A5A2017323), 4) the 4TH BK21 project (Educational Research Group for Platform development of management of emerging infectious disease) funded by the Korean ministry of education (5199990614732).

Figure Legend

Fig 1. Identification of CTCF binding site on EBV genome in SUN719 cell line. A) CTCF enrichment in the EBV genome of SNU719 cells was identified by CTCF ChIP-seq assay. ChIP-seq data in SNU719 cells were aligned to EBV reference genome (NC_007605) for CTCF enrichment. Peak calling identifies 16 significant peaks in ChIP-seq signals. Approximate positions in EBV genome were indicated in the schematic with CTCF binding

582 sites and primer sets used for ChIP RT-qPCR. **B)** Resultant CTCF enrichments identified by
583 ChIP-seq assay were confirmed through the CTCF ChIP-qPCR assay. The ChIP-qPCR was
584 assayed with SNU719 cells using antibody for CTCF. EBV 38,173 primer set was used as
585 negative control. **C)** Like CTCF ChIP-qPCR assay, cohesin subunits such as SMC1 and
586 SMC3 were also tested their enrichment at CTCF BSs by the cohesin ChIP-qPCR assays.

587

588 **Fig 2. Detection of CTCF-DNA interaction using the Monolith NT.115. A)** S13 5' FAM
589 labeled 49-mer primer whose sequence was mutated (Mt S13 primer sets) or not (Wt S13
590 primer sets). **B)** Confirmation of CTCF quality by Western blot assay. CTCF was purified
591 using Sf9 baculovirus protein expression system. Upper panel: Sf9 total protein, lower panel:
592 purified CTCF protein. **C)** CTCF-DNA interaction tested by Microscale thermophoresis
593 (MST) assay. Wt/Mt S13 5' FAM labeled 49-mer primer sets were paired to convert double
594 DNA fragments. MST assays for CTCF binding to Wt/Mt S13 DNA fragments were
595 conducted with 125 nM DNA fragments and 3.12 μM or 6.25 μM CTCF.

596

597 **Fig 3. 4C-plots on EBV genome. A)** The brief 4C experimental procedure and bait positions
598 on EBV genome. Five genomic loci (2 BART, FR, DS/Cp, Qp, LMP) were used as baits. **B)**
599 and **C)** The entire EBV genome was divided into 10-kb windows with each 10 bp sliding, and
600 read numbers indicating associations between the bait regions and 10-kb sections were plotted
601 (top). The experiments are duplicated. **D)** Simple summary of multiple chromatin interactions
602 mediated by CTCF BSs, given to 4C-seq assay data.

603

Fig 4. Confirmation of chromatin interaction by 3C-semi-quantitative (sq)PCR assay. **A)** Sites of *XhoI* restriction sites and 3C-sqPCR primers on EBV genome. **B)** 3C-sqPCR assay using 147K (S14) region as a view primer. EBV genome in SNU719 cells were cut by *XhoI* restriction enzyme, ligated by T4 DNA ligase, and then purified as described previously. Resultant EBV genome DNA was subjected to 3C-sqPCR assay. **C)** 3C-sqPCR assay using 135K (S13) region as a view primer. **D)** Summary of 3C-sqPCR assay data in table. O and o stand for strong and weak chromatin interactions, respectively. x stands for no detection. **E)** A simple diagram to indicate a DNA loop cluster mediated by BARTp CTCF BS associated chromatin interactions in SNU719 cells.

Fig 5. EBV infection assay. A) Schematic diagram of EBV infection assay. HEK293-EBV B(+/-) $S13^{+}$ (Wt) and $S13^{-}$ (Mt) cells were transfected with pCDNA3-BZLF1 and pcDNA3-BALF4. In three days post transfection, supernatants of transfected HEK293-EBV B(+/-) $S13^{+/-}$ (Wt/Mt) cells were harvested and loaded on HEK293 cells freshly cultured on 6-well plate where cell strainer was equipped. EBV in harvested supernatants would infect HEK293 cells for 24 h. After infection, GFP from HEK293 cells infected by EBV was detected in series of time points. **B)** Infection assay of B(-) $S13^{+/-}$ (Wt/Mt) EBVs to HEK293 cells. **C)** Infection assay of B(+/-) $S13^{+/-}$ (Wt/Mt) EBVs to HEK293 cells.

Fig 6. EBV gene expression in BARTp CTCF BS mutant EBVs. A) RT-quantitative (q)PCR assay was conducted to define profiles of EBV gene expression in HEK293-EBV B(-) $S13^{+/-}$ (Wt/Mt) cells. **B)** The mRNA expression profile was defined in HEK293-EBV B(+) $S13^{+/-}$ (Wt/Mt) cells. **C)** Western blot assay to compare EBV protein expressions

627 between HEK293-EBV B(-) $S13^+$ (Wt) and $S13^-$ (Mt) cells. **D)** Western blot assay to compare
628 EBV protein expressions between HEK293-EBV B(+) $S13^+$ (Wt) and $S13^-$ (Mt) cells. **E)**
629 EBNA1 expressions in HEK293-EBV B(+/-) $S13^{+/-}$ (Wt/Mt) cells were compared by
630 immunofluorescence assay. Representive images for interphase nuclei stained with EBNA1
631 and Alexa flour 594 were shown.

632

633 **Fig. 7. CTCF enrichment in HEK293-EBV B(+/-) $S13^{+/-}$ cells. A)** CTCF binding affinities
634 were measured by CTCF ChIP-qPCR assay in HEK293-EBV B(-) $S13^{+/-}$ (Wt/Mt) cells. **B)**
635 CTCF binding affinities were measured by CTCF ChIP-qPCR assay in HEK293-EBV B(+)
636 $S13^{+/-}$ (Wt/Mt) cells. **C)** CTCF ChIP products from HEK293-EBV B(-) $S13^{+/-}$ (Wt/Mt) cells
637 were confirmed their enrichments using sqPCR. **D)** CTCF ChIP products from HEK293-EBV
638 B(+) $S13^{+/-}$ (Wt/Mt) cells were confirmed their enrichments using sqPCR assay.

639

640 **Fig 8. Confirmation of chromatin interaction affected by BARTp CTCF BS mutation.**
641 **A)** and **B)** Sites of *XhoI* restriction sites and 3C primers on EBV genome. EBV genome in
642 HEK293-B(-) $S13^{+/-}$ (Wt/Mt) EBV cells. were cut by *XhoI* restriction enzyme, ligated by T4
643 DNA ligase, and then purified as described previously. Resultant EBV genome DNA was
644 subjected to 3C semi-quantitative PCR assay with view-point primers designed around 147K
645 and 135K, respectively. **C)** Summary of 3C assays. O and o stand for strong and weak
646 chromatin interactions, respectively. X stands for no detection. **D)** Simple diagrams to indicate
647 a DNA loop cluster mediated by BARTp CTCF BS associated chromatin interactions in
648 HEK293-EBV B(+/-) $S13^{+/-}$ (Wt/Mt) cells.

649

Supplemental Fig 1. Construction of HEK293-EBV B(+/-) S13$^-$ cells. A) Schematic diagram of EBV B(+/-) S13$^+$ (Wt/Mt) bacmids. **B)** Sequences introduced at points of recombination to make site-directed mutations in BARTp CTCF BS. **C)** Confirmation of the site-directed mutation in BARTp CTCF BS in EBV B(+) S13$^-$ (Mt) bacmid BY Sanger DNA sequencing. In parallel, EBV B(-) S13$^-$ (Mt) bacmid was also confirmed the mutation by Sanger DNA sequencing (data not shown). **D)** Gel electrophoresis to check EBV genome stabilities of EBV B(+) S13$^-$ (Mt) bacmids by *EcoRI* digestion; EBV B(+) S13$^+$ (Wt) bacmid (lane 1), EBV B(+) S13$^-$ bacmid-*Kan^r* with 1st recombination (lane 2), and EBV B(+) S13$^-$ (Mt) bacmid with 2nd recombination (lane 3). We could not find any loss in EBV B(+) S13$^-$ (Mt) bacmid. In parallel, EBV B(-) S13$^-$ (Mt) bacmid was also confirmed their stabilities without any loss (data not shown). **E)** HEK293 cells were transfected with EBV B(+/-) S13$^{+/-}$ (Wt/Mt) bacmids and selected using hygromycin B to establish HEK293-EBV B(+/-) S13$^{+/-}$ (Wt/Mt) cells. GFP expression were determined in 40 days after hygromycin B selection and several passages. Established HEK293-EBV B(+/-) S13$^{+/-}$ (Wt/Mt) cells were confirmed to maintain their GFP expressions even after several passages.

References

1. Kieff E. Epstein-Barr Virus and Its Replication. 5th ed. Philadelphia, PA: Wolters Kluwer Health/Lippincott/The Williams & Wilkins Co; 2007.
2. Shibata D, Tokunaga M, Uemura Y, Sato E, Tanaka S, Weiss LM. Association of Epstein-Barr virus with undifferentiated gastric carcinomas with intense lymphoid infiltration. Lymphoepithelioma-like carcinoma. The American journal of pathology. 1991;139(3):469-74. Epub 1991/09/01. PubMed PMID: 1653517; PubMed Central PMCID: PMCPMC1886210.
3. Thorley-Lawson DA, Allday MJ. The curious case of the tumour virus: 50 years of Burkitt's lymphoma. Nature Reviews Microbiology. 2008;6:913. doi: 10.1038/nrmicro2015.
4. Hung SC, Kang MS, Kieff E. Maintenance of Epstein-Barr virus (EBV) oriP-based episomes

676 requires EBV-encoded nuclear antigen-1 chromosome-binding domains, which can be replaced by
677 high-mobility group-I or histone H1. Proceedings of the National Academy of Sciences of the
678 United States of America. 2001;98(4):1865-70. Epub 2001/02/15. doi: 10.1073/pnas.031584698.
679 PubMed PMID: 11172042; PubMed Central PMCID: PMCPMC29348.
680 5. Rowe M, Lear AL, Croom-Carter D, Davies AH, Rickinson AB. Three pathways of Epstein-
681 Barr virus gene activation from EBNA1-positive latency in B lymphocytes. J Virol. 1992;66(1):122-
682 31. Epub 1992/01/01. PubMed PMID: 1309242; PubMed Central PMCID: PMCPMC238267.
683 6. Chen H-S, Lu F, Lieberman PM. Epigenetic regulation of EBV and KSHV latency. Current
684 opinion in virology. 2013;3(3):251-9. Epub 04/16. doi: 10.1016/j.coviro.2013.03.004. PubMed PMID:
685 23601957.
686 7. Shibata D, Weiss LM. Epstein-Barr virus-associated gastric adenocarcinoma. The American
687 journal of pathology. 1992;140(4):769-74. Epub 1992/04/01. PubMed PMID: 1314023; PubMed
688 Central PMCID: PMCPMC1886378.
689 8. Nishikawa J, Yoshiyama H, Iizasa H, Kanehiro Y, Nakamura M, Nishimura J, et al. Epstein-
690 barr virus in gastric carcinoma. Cancers. 2014;6(4):2259-74. doi: 10.3390/cancers6042259. PubMed
691 PMID: 25386788.
692 9. Takada K. Epstein-Barr virus and gastric carcinoma. Molecular pathology : MP.
693 2000;53(5):255-61. PubMed PMID: 11091849.
694 10. Imai S, Koizumi S, Sugiura M, Tokunaga M, Uemura Y, Yamamoto N, et al. Gastric
695 carcinoma: monoclonal epithelial malignant cells expressing Epstein-Barr virus latent infection
696 protein. Proceedings of the National Academy of Sciences of the United States of America.
697 1994;91(19):9131-5. Epub 1994/09/13. PubMed PMID: 8090780; PubMed Central PMCID:
698 PMCPMC44761.
699 11. Chen H, Huang J, Wu FY, Liao G, Hutt-Fletcher L, Hayward SD. Regulation of expression
700 of the Epstein-Barr virus BamHI-A rightward transcripts. J Virol. 2005;79(3):1724-33. Epub
701 2005/01/15. doi: 10.1128/jvi.79.3.1724-1733.2005. PubMed PMID: 15650197; PubMed Central
702 PMCID: PMCPMC544122.
703 12. Chen HL, Lung MM, Sham JS, Choy DT, Griffin BE, Ng MH. Transcription of BamHI-A
704 region of the EBV genome in NPC tissues and B cells. Virology. 1992;191(1):193-201. Epub
705 1992/11/01. PubMed PMID: 1329317.
706 13. Cheung ST, Huang DP, Hui AB, Lo KW, Ko CW, Tsang YS, et al. Nasopharyngeal carcinoma
707 cell line (C666-1) consistently harbouring Epstein-Barr virus. International journal of cancer.
708 1999;83(1):121-6. Epub 1999/08/17. PubMed PMID: 10449618.
709 14. Cullen BR. Transcription and processing of human microRNA precursors. Molecular cell.
710 2004;16(6):861-5. Epub 2004/12/22. doi: 10.1016/j.molcel.2004.12.002. PubMed PMID: 15610730.
711 15. Gilligan K, Sato H, Rajadurai P, Busson P, Young L, Rickinson A, et al. Novel transcription
712 from the Epstein-Barr virus terminal EcoRI fragment, DIJhet, in a nasopharyngeal carcinoma. J Virol.

1990;64(10):4948-56. Epub 1990/10/01. PubMed PMID: 2168978; PubMed Central PMCID: PMCPMC247986.

16. Karran L, Gao Y, Smith PR, Griffin BE. Expression of a family of complementary-strand transcripts in Epstein-Barr virus-infected cells. Proceedings of the National Academy of Sciences of the United States of America. 1992;89(17):8058-62. Epub 1992/09/01. PubMed PMID: 1325642; PubMed Central PMCID: PMCPMC49855.

17. Edwards RH, Marquitz AR, Raab-Traub N. Epstein-Barr virus BART microRNAs are produced from a large intron prior to splicing. J Virol. 2008;82(18):9094-106. Epub 2008/07/11. doi: 10.1128/jvi.00785-08. PubMed PMID: 18614630; PubMed Central PMCID: PMCPMC2546912.

18. Raab-Traub N, Dambaugh T, Kieff E. DNA of Epstein-Barr virus VIII: B95-8, the previous prototype, is an unusual deletion derivative. Cell. 1980;22(1 Pt 1):257-67. Epub 1980/11/01. PubMed PMID: 6253079.

19. Kim DN, Chae H-S, Oh ST, Kang J-H, Park CH, Park WS, et al. Expression of viral microRNAs in Epstein-Barr virus-associated gastric carcinoma. Journal of virology. 2007;81(2):1033-6. Epub 11/01. doi: 10.1128/JVI.02271-06. PubMed PMID: 17079300.

20. Zhu JY, Pfuhl T, Motsch N, Barth S, Nicholls J, Grasser F, et al. Identification of novel Epstein-Barr virus microRNA genes from nasopharyngeal carcinomas. J Virol. 2009;83(7):3333-41. Epub 2009/01/16. doi: 10.1128/jvi.01689-08. PubMed PMID: 19144710; PubMed Central PMCID: PMCPMC2655542.

21. Choy EY, Siu KL, Kok KH, Lung RW, Tsang CM, To KF, et al. An Epstein-Barr virus-encoded microRNA targets PUMA to promote host cell survival. The Journal of experimental medicine. 2008;205(11):2551-60. Epub 2008/10/08. doi: 10.1084/jem.20072581. PubMed PMID: 18838543; PubMed Central PMCID: PMCPMC2571930.

22. Marquitz AR, Mathur A, Shair KHY, Raab-Traub N. Infection of Epstein–Barr virus in a gastric carcinoma cell line induces anchorage independence and global changes in gene expression. Proceedings of the National Academy of Sciences. 2012;109(24):9593.

23. Bushey AM, Dorman ER, Corces VG. Chromatin insulators: regulatory mechanisms and epigenetic inheritance. Molecular cell. 2008;32(1):1-9. Epub 2008/10/15. doi: 10.1016/j.molcel.2008.08.017. PubMed PMID: 18851828; PubMed Central PMCID: PMCPMC2576288.

24. West AG, Gaszner M, Felsenfeld G. Insulators: many functions, many mechanisms. Genes & development. 2002;16(3):271-88. Epub 2002/02/05. doi: 10.1101/gad.954702. PubMed PMID: 11825869.

25. Wallace JA, Felsenfeld G. We gather together: insulators and genome organization. Current opinion in genetics & development. 2007;17(5):400-7. Epub 2007/10/05. doi: 10.1016/j.gde.2007.08.005. PubMed PMID: 17913488; PubMed Central PMCID: PMCPMC2215060.

26. Capelson M, Corces VG. Boundary elements and nuclear organization. Biology of the cell.

2004;96(8):617-29. Epub 2004/11/03. doi: 10.1016/j.biolcel.2004.06.004. PubMed PMID: 15519696.

27. Filippova GN, Fagerlie S, Klenova EM, Myers C, Dehner Y, Goodwin G, et al. An exceptionally conserved transcriptional repressor, CTCF, employs different combinations of zinc fingers to bind diverged promoter sequences of avian and mammalian c-myc oncogenes. Molecular and cellular biology. 1996;16(6):2802-13. Epub 1996/06/01. PubMed PMID: 8649389; PubMed Central PMCID: PMCPMC231272.

28. Klenova EM, Nicolas RH, Paterson HF, Carne AF, Heath CM, Goodwin GH, et al. CTCF, a conserved nuclear factor required for optimal transcriptional activity of the chicken c-myc gene, is an 11-Zn-finger protein differentially expressed in multiple forms. Molecular and cellular biology. 1993;13(12):7612-24. Epub 1993/12/01. PubMed PMID: 8246978; PubMed Central PMCID: PMCPMC364833.

29. Lobanenkov VV, Nicolas RH, Adler VV, Paterson H, Klenova EM, Polotskaja AV, et al. A novel sequence-specific DNA binding protein which interacts with three regularly spaced direct repeats of the CCCTC-motif in the 5'-flanking sequence of the chicken c-myc gene. Oncogene. 1990;5(12):1743-53. Epub 1990/12/01. PubMed PMID: 2284094.

30. Ohlsson R, Renkawitz R, Lobanenkov V. CTCF is a uniquely versatile transcription regulator linked to epigenetics and disease. Trends in genetics : TIG. 2001;17(9):520-7. Epub 2001/08/30. PubMed PMID: 11525835.

31. Rubio ED, Reiss DJ, Welcsh PL, Disteche CM, Filippova GN, Baliga NS, et al. CTCF physically links cohesin to chromatin. Proceedings of the National Academy of Sciences of the United States of America. 2008;105(24):8309-14. Epub 2008/06/14. doi: 10.1073/pnas.0801273105. PubMed PMID: 18550811; PubMed Central PMCID: PMCPMC2448833.

32. Stedman W, Kang H, Lin S, Kissil JL, Bartolomei MS, Lieberman PM. Cohesins localize with CTCF at the KSHV latency control region and at cellular c-myc and H19/Igf2 insulators. The EMBO journal. 2008;27(4):654-66. Epub 2008/01/26. doi: 10.1038/emboj.2008.1. PubMed PMID: 18219272; PubMed Central PMCID: PMCPMC2262040.

33. Wendt KS, Yoshida K, Itoh T, Bando M, Koch B, Schirghuber E, et al. Cohesin mediates transcriptional insulation by CCCTC-binding factor. Nature. 2008;451(7180):796-801. Epub 2008/02/01. doi: 10.1038/nature06634. PubMed PMID: 18235444.

34. Arvey A, Tempera I, Tsai K, Chen HS, Tikhmyanova N, Klichinsky M, et al. An atlas of the Epstein-Barr virus transcriptome and epigenome reveals host-virus regulatory interactions. Cell host & microbe. 2012;12(2):233-45. Epub 2012/08/21. doi: 10.1016/j.chom.2012.06.008. PubMed PMID: 22901543; PubMed Central PMCID: PMCPMC3424516.

35. Day L, Chau CM, Nebozhyn M, Rennekamp AJ, Showe M, Lieberman PM. Chromatin profiling of Epstein-Barr virus latency control region. J Virol. 2007;81(12):6389-401. Epub 2007/04/06. doi: 10.1128/jvi.02172-06. PubMed PMID: 17409162; PubMed Central PMCID: PMCPMC1900095.

787 36. Holdorf MM, Cooper SB, Yamamoto KR, Miranda JJ. Occupancy of chromatin organizers
788 in the Epstein-Barr virus genome. Virology. 2011;415(1):1-5. Epub 2011/05/10. doi:
789 10.1016/j.virol.2011.04.004. PubMed PMID: 21550623; PubMed Central PMCID: PMCPMC3808970.
790 37. Choi SJ, Ryu E, Lee S, Huh S, Shin YS, Kang BW, et al. Adenosine Induces EBV Lytic
791 Reactivation through ADORA1 in EBV-Associated Gastric Carcinoma. Int J Mol Sci. 2019;20(6). doi:
792 10.3390/ijms20061286. PubMed PMID: 30875759; PubMed Central PMCID: PMCPMC6471230.
793 38. Kanda T, Miyata M, Kano M, Kondo S, Yoshizaki T, Iizasa H. Clustered microRNAs of the
794 Epstein-Barr virus cooperatively downregulate an epithelial cell-specific metastasis suppressor. J
795 Virol. 2015;89(5):2684-97. doi: 10.1128/JVI.03189-14. PubMed PMID: 25520514; PubMed Central
796 PMCID: PMCPMC4325718.
797 39. Heinz S, Benner C, Spann N, Bertolino E, Lin YC, Laslo P, et al. Simple combinations of
798 lineage-determining transcription factors prime cis-regulatory elements required for macrophage
799 and B cell identities. Molecular cell. 2010;38(4):576-89. Epub 2010/06/02. doi:
800 10.1016/j.molcel.2010.05.004. PubMed PMID: 20513432; PubMed Central PMCID:
801 PMCPMC2898526.
802 40. Kim KD, Tanizawa H, De Leo A, Vladimirova O, Kossenkov A, Lu F, et al. Epigenetic
803 specifications of host chromosome docking sites for latent Epstein-Barr virus. Nat Commun.
804 2020;11(1):877. doi: 10.1038/s41467-019-14152-8. PubMed PMID: 32054837; PubMed Central
805 PMCID: PMCPMC7018943.
806 41. Tempera I, Wiedmer A, Dheekollu J, Lieberman PM. CTCF prevents the epigenetic drift of
807 EBV latency promoter Qp. PLoS Pathog. 2010;6(8):e1001048. doi: 10.1371/journal.ppat.1001048.
808 PubMed PMID: 20730088; PubMed Central PMCID: PMCPMC2921154.
809 42. Rao SS, Huntley MH, Durand NC, Stamenova EK, Bochkov ID, Robinson JT, et al. A 3D
810 map of the human genome at kilobase resolution reveals principles of chromatin looping. Cell.
811 2014;159(7):1665-80. doi: 10.1016/j.cell.2014.11.021. PubMed PMID: 25497547; PubMed Central
812 PMCID: PMCPMC5635824.
813 43. Chen HS, Martin KA, Lu F, Lupey LN, Mueller JM, Lieberman PM, et al. Epigenetic
814 deregulation of the LMP1/LMP2 locus of Epstein-Barr virus by mutation of a single CTCF-cohesin
815 binding site. Journal of virology. 2014;88(3):1703-13. doi: 10.1128/JVI.02209-13. PubMed PMID:
816 24257606; PubMed Central PMCID: PMCPMC3911611.
817 44. Tempera I, Klichinsky M, Lieberman PM. EBV latency types adopt alternative chromatin
818 conformations. PLoS Pathog. 2011;7(7):e1002180. doi: 10.1371/journal.ppat.1002180. PubMed
819 PMID: 21829357; PubMed Central PMCID: PMCPMC3145795.
820 45. Choi SJ, Jung SW, Huh S, Cho H, Kang H. Phylogenetic comparison of Epstein-Barr virus
821 genomes. J Microbiol. 2018;56(8):525-33. doi: 10.1007/s12275-018-8039-x. PubMed PMID:
822 29948828.
823 46. Chau CM, Zhang XY, McMahon SB, Lieberman PM. Regulation of Epstein-Barr virus latency

824 type by the chromatin boundary factor CTCF. J Virol. 2006;80(12):5723-32. doi: 10.1128/JVI.00025-
825 06. PubMed PMID: 16731911; PubMed Central PMCID: PMCPMC1472585.
826 47. Holwerda S, de Laat W. Chromatin loops, gene positioning, and gene expression. Front
827 Genet. 2012;3:217. doi: 10.3389/fgene.2012.00217. PubMed PMID: 23087710; PubMed Central
828 PMCID: PMCPMC3473233.
829 48. Puglielli MT, Woisetschlaeger M, Speck SH. oriP is essential for EBNA gene promoter
830 activity in Epstein-Barr virus-immortalized lymphoblastoid cell lines. J Virol. 1996;70(9):5758-68.
831 doi: 10.1128/JVI.70.9.5758-5768.1996. PubMed PMID: 8709191; PubMed Central PMCID:
832 PMCPMC190589.
833 49. Kang H, Wiedmer A, Yuan Y, Robertson E, Lieberman PM. Coordination of KSHV latent
834 and lytic gene control by CTCF-cohesin mediated chromosome conformation. PLoS Pathog.
835 2011;7(8):e1002140. doi: 10.1371/journal.ppat.1002140. PubMed PMID: 21876668; PubMed Central
836 PMCID: PMCPMC3158054.
837 50. Weth O, Renkawitz R. CTCF function is modulated by neighboring DNA binding factors.
838 Biochem Cell Biol. 2011;89(5):459-68. doi: 10.1139/o11-033. PubMed PMID: 21895576.
839 51. Herold M, Bartkuhn M, Renkawitz R. CTCF: insights into insulator function during
840 development. Development. 2012;139(6):1045-57. doi: 10.1242/dev.065268. PubMed PMID:
841 22354838.
842 52. Moquin SA, Thomas S, Whalen S, Warburton A, Fernandez SG, McBride AA, et al. The
843 Epstein-Barr Virus Episome Maneuvers between Nuclear Chromatin Compartments during
844 Reactivation. J Virol. 2018;92(3). doi: 10.1128/JVI.01413-17. PubMed PMID: 29142137; PubMed
845 Central PMCID: PMCPMC5774889.
846 53. Campbell M, Watanabe T, Nakano K, Davis RR, Lyu Y, Tepper CG, et al. KSHV episomes
847 reveal dynamic chromatin loop formation with domain-specific gene regulation. Nat Commun.
848 2018;9(1):49. doi: 10.1038/s41467-017-02089-9. PubMed PMID: 29302027; PubMed Central PMCID:
849 PMCPMC5754359.

850

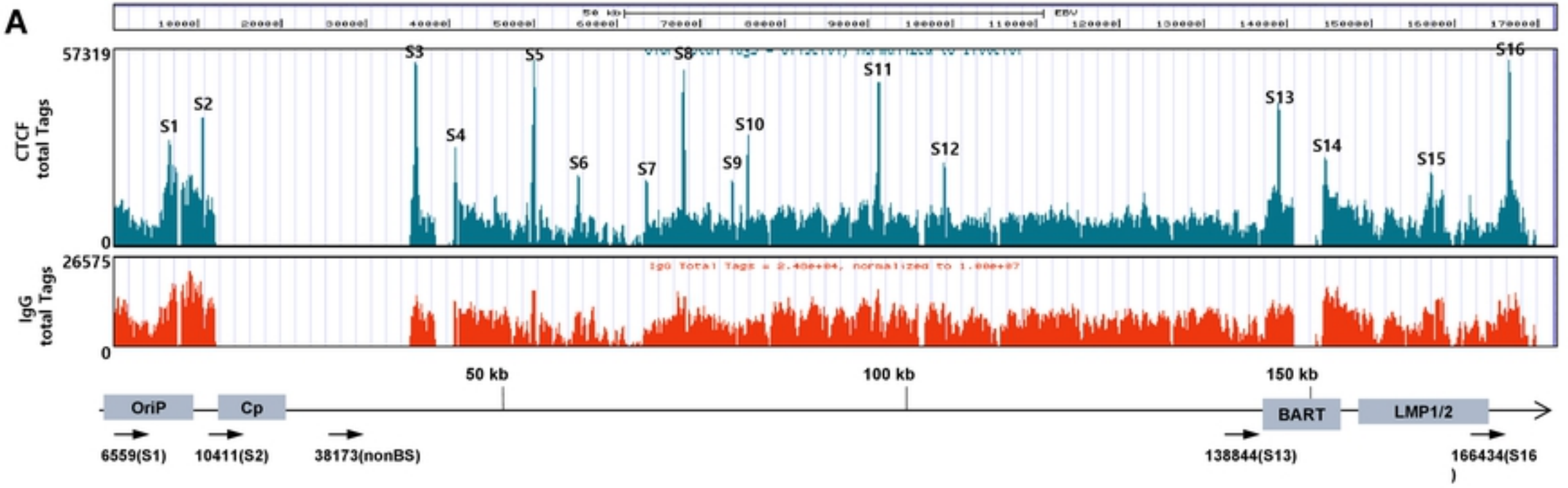
A
CTCF total Tags
57319
0
S1
S2
S3
S4
S5
S6
S7
S8
S9
S10
S11
S12
S13
S14
S15
S16
IgG total Tags
26575
0
50 kb
100 kb
150 kb
OriP
Cp
BART
LMP1/2
6559(S1)
10411(S2)
38173(nonBS)
138844(S13)
166434(S16)

Fig. 1-1.

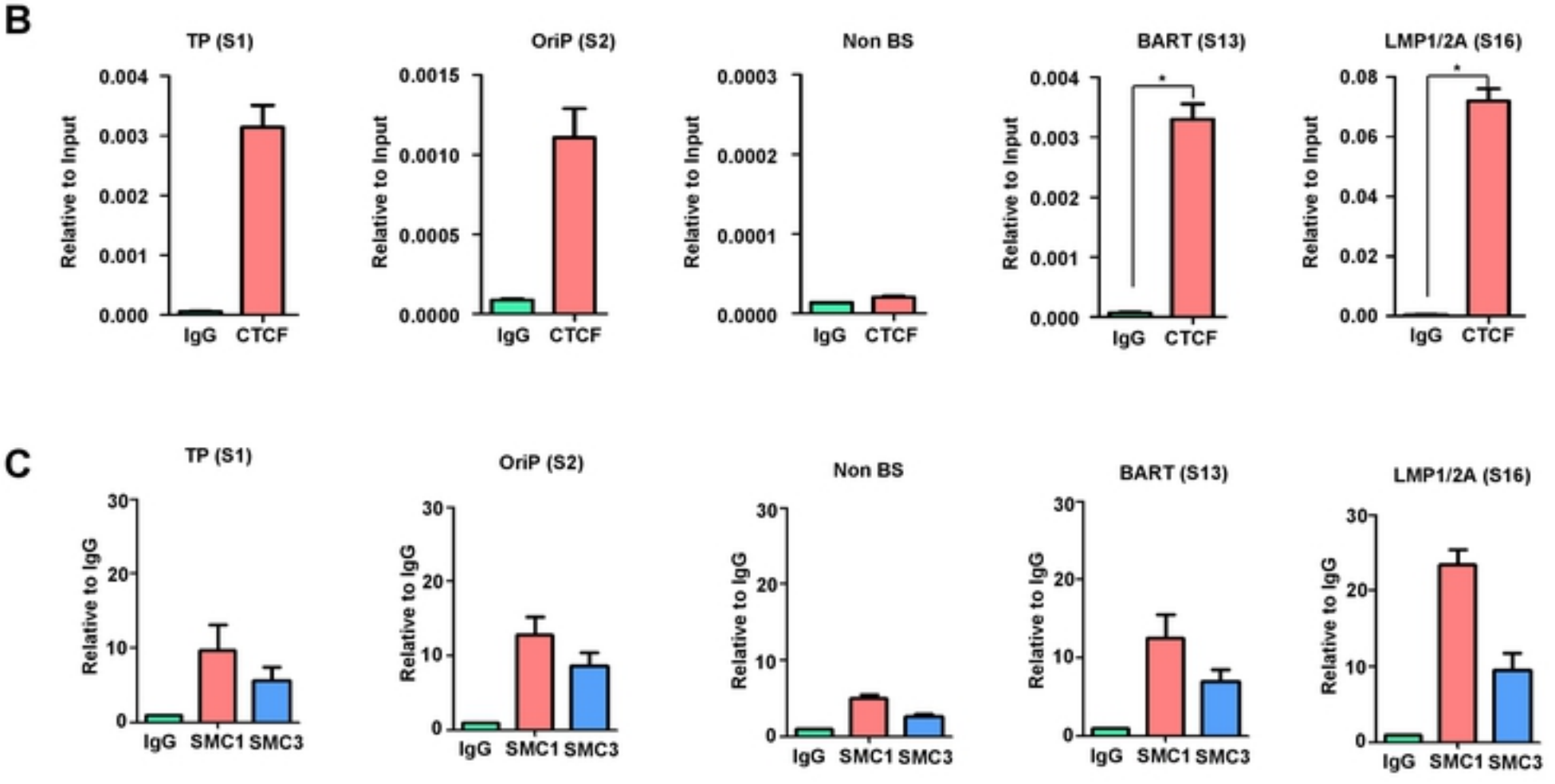
B
TP (S1)
OriP (S2)
Non BS
BART (S13)
LMP1/2A (S16)
Relative to Input
IgG
CTCF
C
Relative to IgG
IgG
SMC1
SMC3

Fig. 1-2.

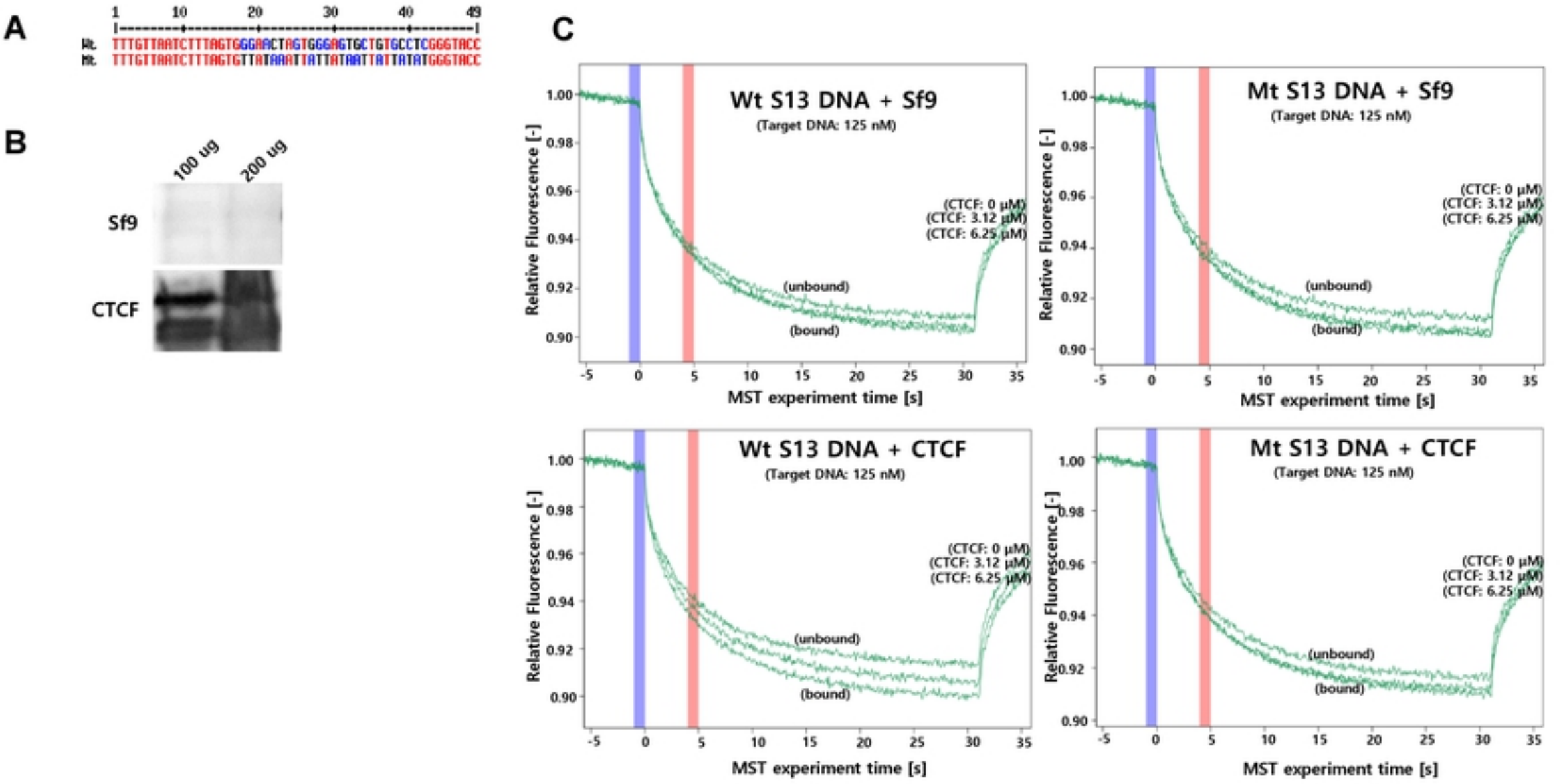
A
1 10 20 30 40 49
Wt. TTTGTTAATCTTTAGTGGGAACTAGTGGGAGTGCTGTGCCTCGGGTACC
Mt. TTTGTTAATCTTTAGTGTTATAAATTATTATAATTATTATATGGGTACC
B
100 ug
200 ug
Sf9
CTCF
C
Wt S13 DNA + Sf9
(Target DNA: 125 nM)
Mt S13 DNA + Sf9
(Target DNA: 125 nM)
Wt S13 DNA + CTCF
(Target DNA: 125 nM)
Mt S13 DNA + CTCF
(Target DNA: 125 nM)
Relative Fluorescence [-]
MST experiment time [s]
(CTCF: 0 μM)
(CTCF: 3.12 μM)
(CTCF: 6.25 μM)
(unbound)
(bound)

Fig. 2.

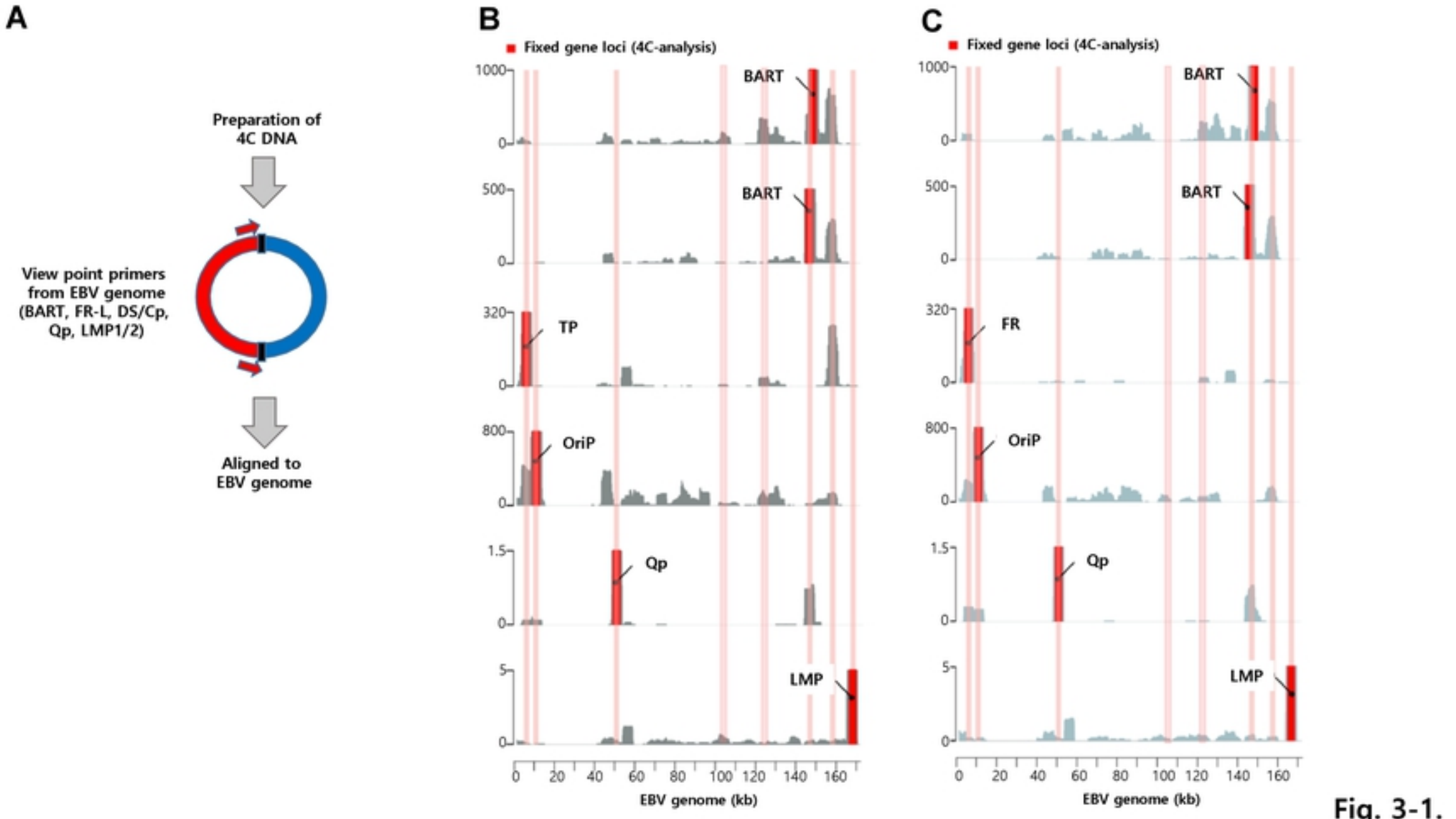
A
Preparation of 4C DNA
View point primers from EBV genome (BART, FR-L, DS/Cp, Qp, LMP1/2)
Aligned to EBV genome
B
Fixed gene loci (4C-analysis)
BART
BART
TP
OriP
Qp
LMP
EBV genome (kb)
C
Fixed gene loci (4C-analysis)
BART
BART
FR
OriP
Qp
LMP
EBV genome (kb)

Fig. 3-1.

D


S12
S1
S13
S15
S12
S12
S5
S2
S1
S15
S1
S2
S5
S14
S1
S2
S16
S4
S 13
S 15

Fig. 3-2.

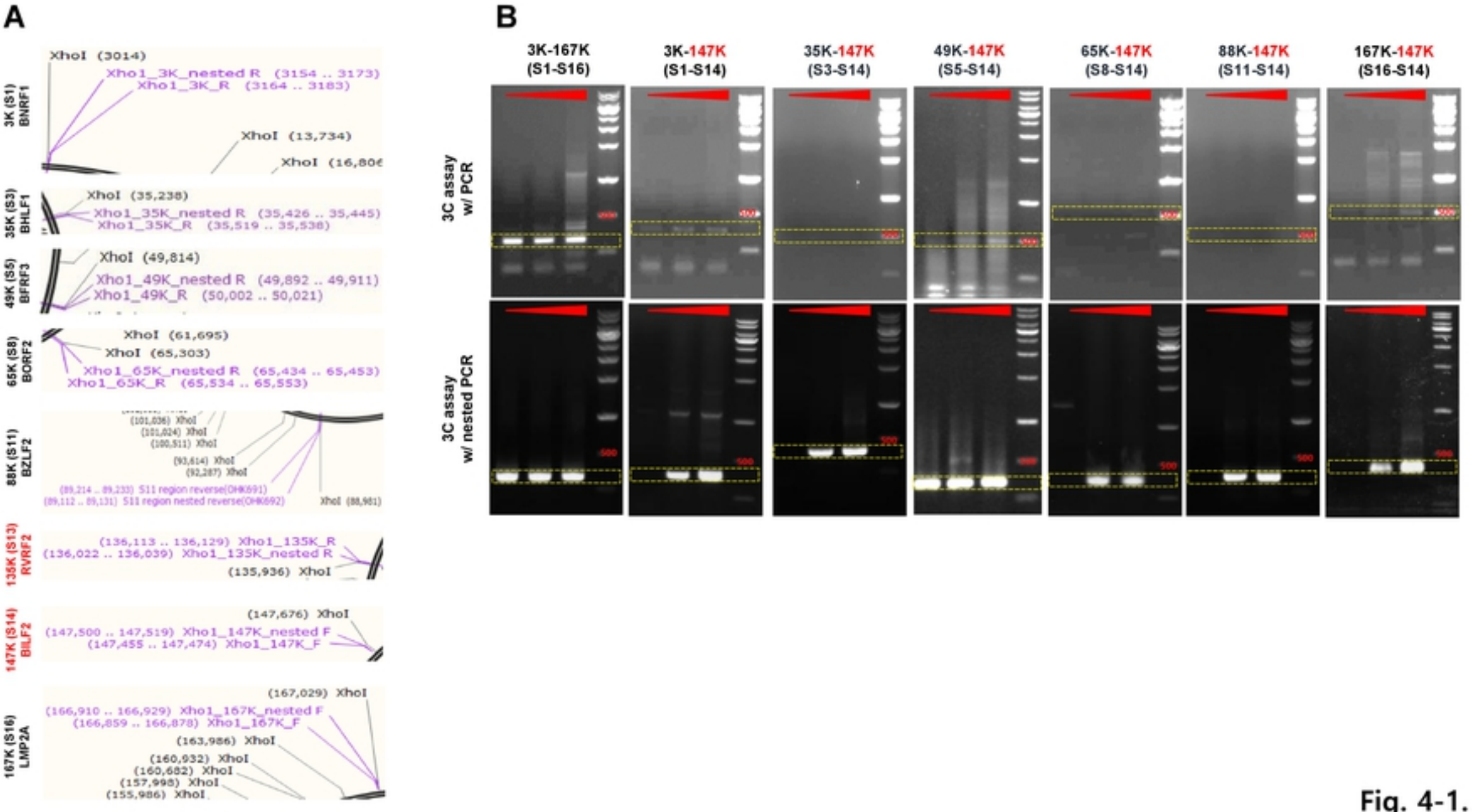
A
3K (S1) BNRF1
XhoI (3014)
Xho1_3K_nested R (3154 .. 3173)
Xho1_3K_R (3164 .. 3183)
XhoI (13,734)
XhoI (16,80
35K (S3) BHLF1
XhoI (35,238)
Xho1_35K_nested R (35,426 .. 35,445)
Xho1_35K_R (35,519 .. 35,538)
49K (S5) BFRF3
XhoI (49,814)
Xho1_49K_nested R (49,892 .. 49,911)
Xho1_49K_R (50,002 .. 50,021)
65K (S8) BORF2
XhoI (61,695)
XhoI (65,303)
Xho1_65K_nested R (65,434 .. 65,453)
Xho1_65K_R (65,534 .. 65,553)
88K (S11) BZLF2
(101,036) XhoI
(101,024) XhoI
(100,511) XhoI
(93,614) XhoI
(92,287) XhoI
(89,214 .. 89,233) S11 region reverse(OHK691)
(89,112 .. 89,131) S11 region nested reverse(OHK692)
XhoI (88,981)
135K (S13) RVRF2
(136,113 .. 136,129) Xho1_135K_R
(136,022 .. 136,039) Xho1_135K_nested R
(135,936) XhoI
147K (S14) BILF2
(147,676) XhoI
(147,500 .. 147,519) Xho1_147K_nested F
(147,455 .. 147,474) Xho1_147K_F
167K (S16) LMP2A
(167,029) XhoI
(166,910 .. 166,929) Xho1_167K_nested F
(166,859 .. 166,878) Xho1_167K_F
(163,986) XhoI
(160,932) XhoI
(160,682) XhoI
(157,995) XhoI
(155,986) XhoI
B
3K-167K (S1-S16)
3K-147K (S1-S14)
35K-147K (S3-S14)
49K-147K (S5-S14)
65K-147K (S8-S14)
88K-147K (S11-S14)
167K-147K (S16-S14)
3C assay w/ PCR
3C assay w/ nested PCR
500

Fig. 4-1.

C

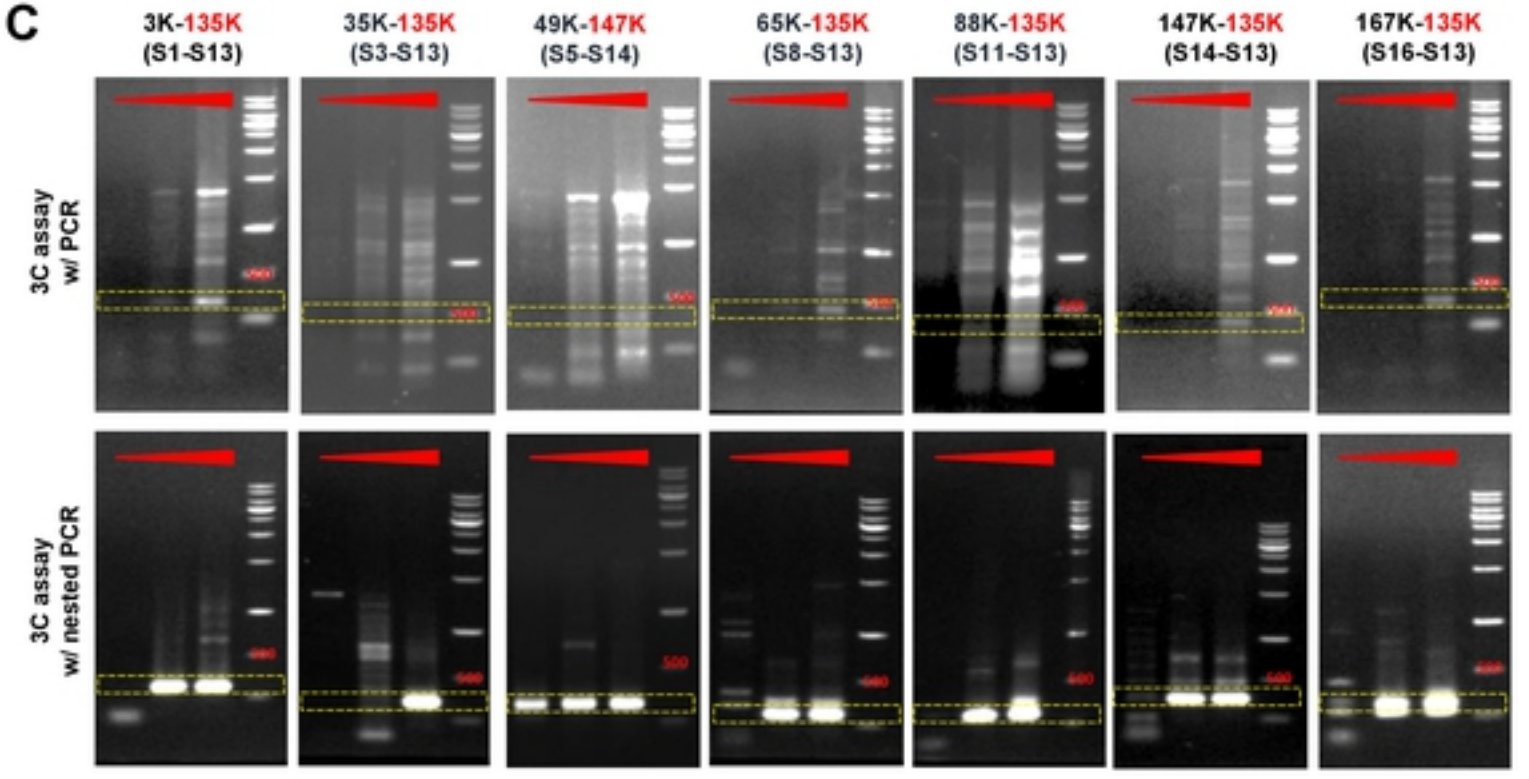

E

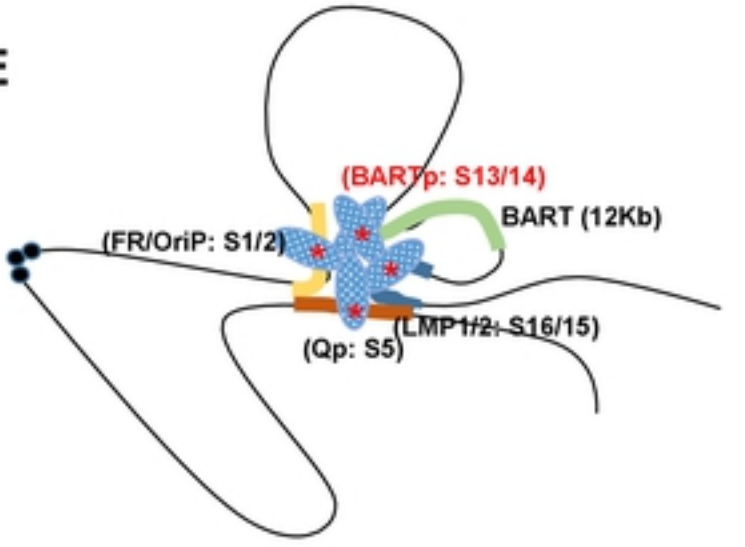

D

3K-167K		3K (S1)	35K (S3)	49K (S5)	65K (S8)	88K (S11)	135K (S13)	147K (S14)	167K (S16)
OOO	147K (S14)	ooo	xxx	xoo	xxx	xxx	xxo		xxO
OOO	135K (S13)	xxO	xxx	xxo	xxo	xxx		xxo	xxo

Fig. 4-2.

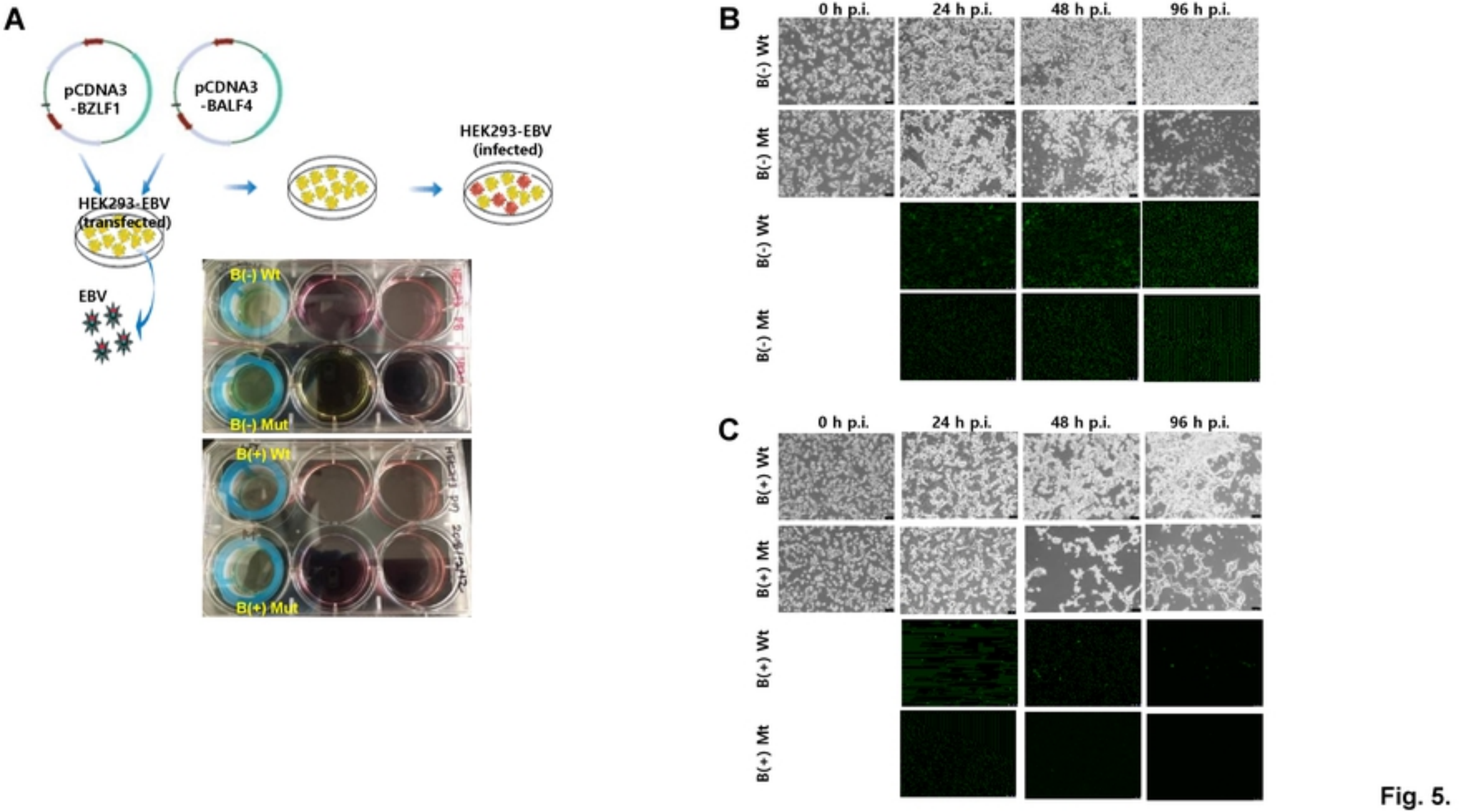
A
pCDNA3
-BZLF1
pCDNA3
-BALF4
HEK293-EBV
(transfected)
HEK293-EBV
(infected)
EBV
B(-) Wt
B(-) Mut
B(+) Wt
B(+) Mut
B
0 h p.i.
24 h p.i.
48 h p.i.
96 h p.i.
B(-) Wt
B(-) Mt
B(-) Wt
B(-) Mt
C
0 h p.i.
24 h p.i.
48 h p.i.
96 h p.i.
B(+) Wt
B(+) Mt
B(+) Wt
B(+) Mt

Fig. 5.

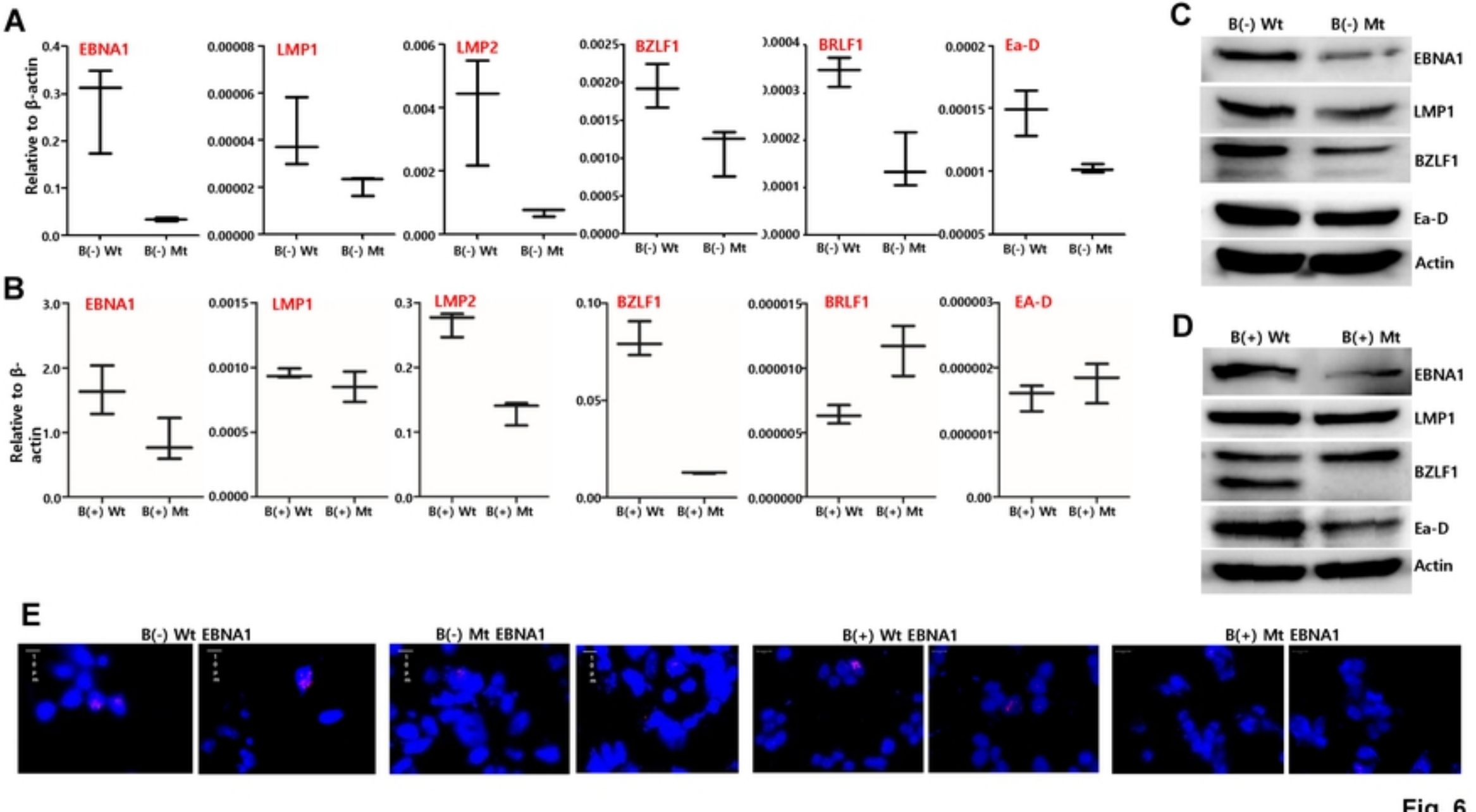
A
EBNA1
LMP1
LMP2
BZLF1
BRLF1
Ea-D
Relative to β-actin
B(-) Wt
B(-) Mt
B
EBNA1
LMP1
LMP2
BZLF1
BRLF1
EA-D
Relative to β-actin
B(+) Wt
B(+) Mt
C
B(-) Wt
B(-) Mt
EBNA1
LMP1
BZLF1
Ea-D
Actin
D
B(+) Wt
B(+) Mt
EBNA1
LMP1
BZLF1
Ea-D
Actin
E
B(-) Wt EBNA1
B(-) Mt EBNA1
B(+) Wt EBNA1
B(+) Mt EBNA1

Fig. 6.

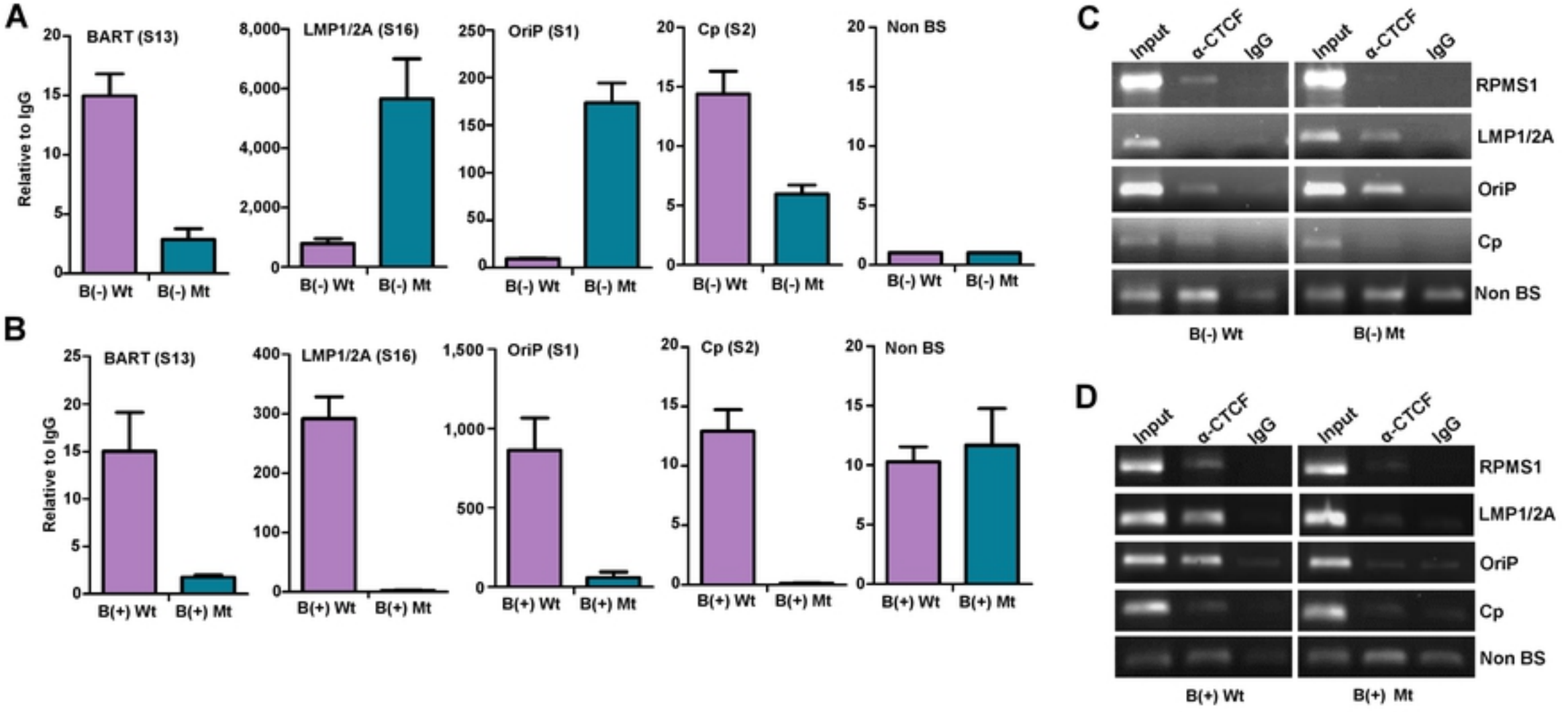
A
BART (S13)
LMP1/2A (S16)
OriP (S1)
Cp (S2)
Non BS
Relative to IgG
B(-) Wt
B(-) Mt
B
BART (S13)
LMP1/2A (S16)
OriP (S1)
Cp (S2)
Non BS
Relative to IgG
B(+) Wt
B(+) Mt
C
Input
α-CTCF
IgG
RPMS1
LMP1/2A
OriP
Cp
Non BS
B(-) Wt
B(-) Mt
D
Input
α-CTCF
IgG
RPMS1
LMP1/2A
OriP
Cp
Non BS
B(+) Wt
B(+) Mt

Fig. 7.

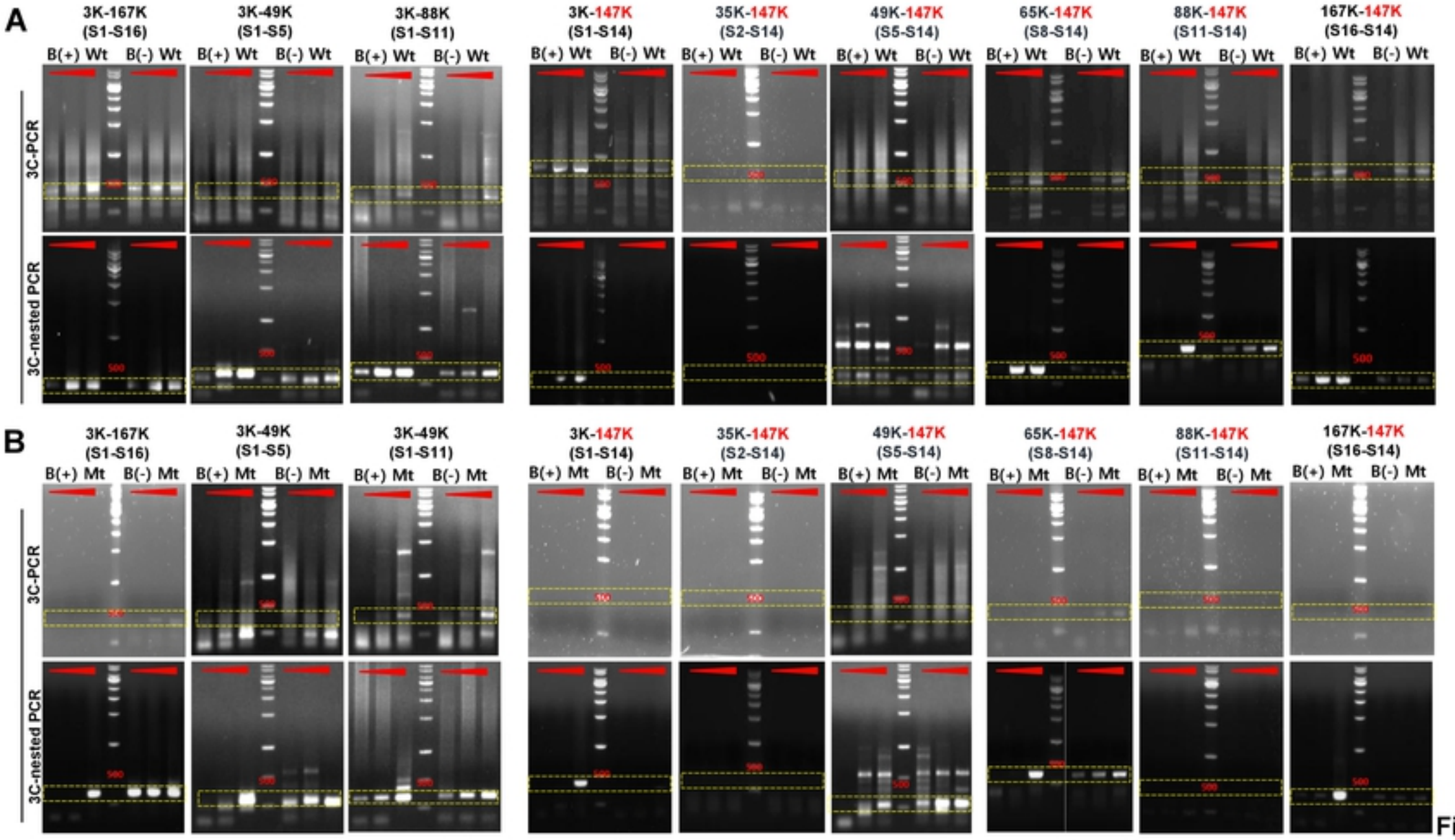
A
3K-167K (S1-S16)
3K-49K (S1-S5)
3K-88K (S1-S11)
3K-147K (S1-S14)
35K-147K (S2-S14)
49K-147K (S5-S14)
65K-147K (S8-S14)
88K-147K (S11-S14)
167K-147K (S16-S14)
B(+) Wt
B(-) Wt
3C-PCR
3C-nested PCR
500
B
3K-167K (S1-S16)
3K-49K (S1-S5)
3K-49K (S1-S11)
3K-147K (S1-S14)
35K-147K (S2-S14)
49K-147K (S5-S14)
65K-147K (S8-S14)
88K-147K (S11-S14)
167K-147K (S16-S14)
B(+) Mt
B(-) Mt
3C-PCR
3C-nested PCR
500

Fig. 8-1

C

	3K-167K		3K-49K		3K-88K		3K-147K		35K-147K		49K-147K		65K-147K		88K-147K		167K-147K	
B(+) Wt	oOO		xxo		xoo		oOO		xxx		xxo		xoO		xxo		xoO	
B(-) Wt		oOO		xxx		xoO		ooo		xxx		xxo		xoo		xxo		xoo
B(+) Mt	xxx		xxx		xoO		xxx		xxx		xxx		xxx		xxx		xxx	
B(-) Mt		xoo		xxx		xoO		xxx		xxx		xxx		xoo		xxx		xxx

D

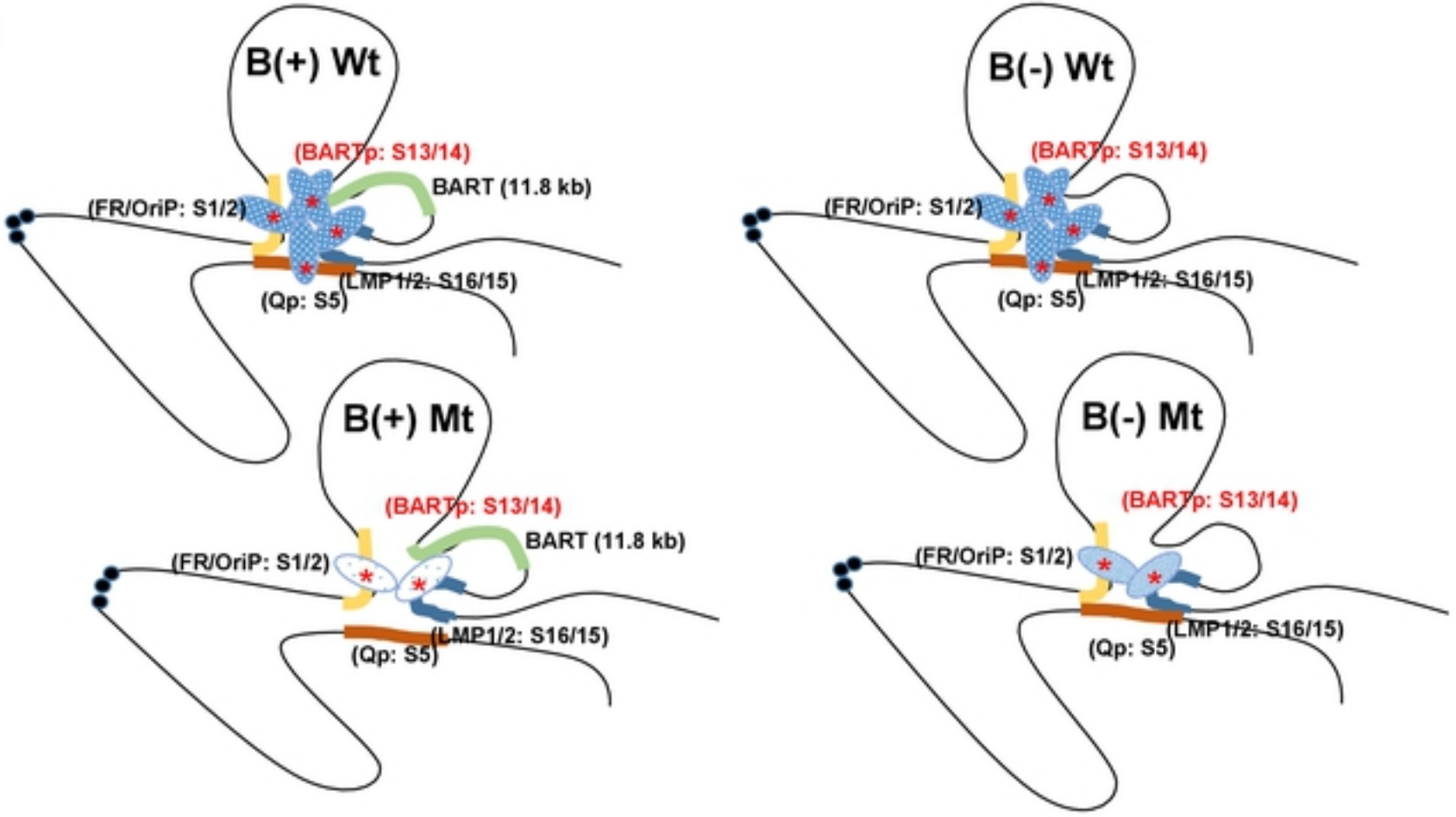

Fig. 8-2

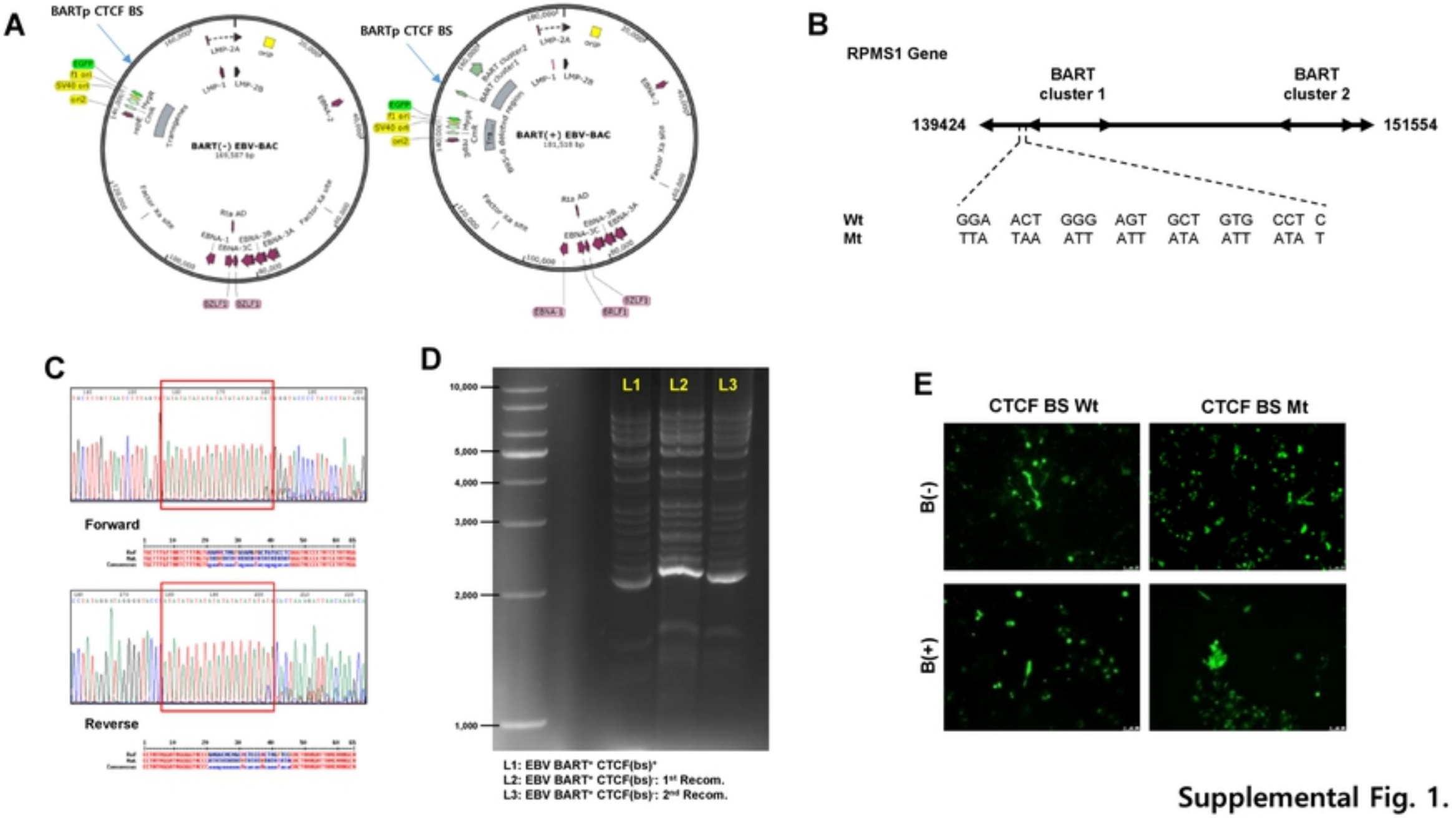

Supplemental Fig. 1.